

Grant Agreement no: 817669

Acronym: MEESO

Project title: Ecologically and economically sustainable mesopelagic fisheries

H2020 project  
Call: H2020-BG-2018-2020 (Blue Growth)  
Topic: LC-BG-03-2018

Starting date: September 1, 2019  
Duration: 48 months

D2.1

Title:

Report on the implementation of acoustical, optical and catch methods for enhanced identification and biomass estimation of mesopelagic species

Date:

Organization name of lead participant for this deliverable:  
IMR

Dissemination level		
PU	Public	X
CO	Confidential, only for members of the consortium (incl the Commission Services)	



Deliverable number:	D2.1
Deliverable title:	Report on the implementation of acoustical, optical and catch methods for enhanced identification and biomass estimation of mesopelagic species
Work package:	WP2
Lead participant:	IMR

Authors		
Name	Organisation	E-mail
Mette Dalgaard Agersted	IMR	<a href="mailto:mette.dalgaard.agersted@hi.no">mette.dalgaard.agersted@hi.no</a>
Birkir Bárðarson	MFRI	<a href="mailto:Birkir.bardarson@hafogvatn.is">Birkir.bardarson@hafogvatn.is</a>
Guillermo Boyra	AZTI	<a href="mailto:gboyra@azti.es">gboyra@azti.es</a>
Babak Khodabandelloo	IMR	<a href="mailto:Babak.Khodabandelloo@hi.no">Babak.Khodabandelloo@hi.no</a>
Thor A. Klevjer*	IMR	<a href="mailto:thor.klevjer@hi.no">thor.klevjer@hi.no</a>
Webjørn Melle	IMR	<a href="mailto:webjoern.melle@hi.no">webjoern.melle@hi.no</a>
Shale Rosen	IMR	<a href="mailto:Shale.rosen@hi.no">Shale.rosen@hi.no</a>
Teresa Silva	MFRI	<a href="mailto:teresa.silva@hafogvatn.is">teresa.silva@hafogvatn.is</a>
Espen Strand	IMR	<a href="mailto:espen.strand@hi.no">espen.strand@hi.no</a>
Kjetil Geitsund Thorvaldsen	DTU	<a href="mailto:kjgth@aqu.dtu.dk">kjgth@aqu.dtu.dk</a>
Melanie Underwood	IMR	<a href="mailto:Melanie.underwood@hi.no">Melanie.underwood@hi.no</a>
Alina Wiczorek	MI	<a href="mailto:Alina.Wiczorek@Marine.ie">Alina.Wiczorek@Marine.ie</a>

\*corresponding authors

Keywords
Mesopelagic resources, Acoustic survey, Trawl survey, methods, quantification



## Executive Summary

This deliverable reports on efforts, methods and techniques implemented and used by the MEESO partners to improve quantification of abundances and biomasses in the mesopelagic zone.

The work reported here has been focused on application of the relatively new acoustic broadband technology for measuring acoustic properties of mesopelagic organisms. The examples provided shows that this technology is promising when it comes to identifying (Chapter 3.2) and quantifying (Chapter 3.3) the abundance of mesopelagic organisms. The obtained results are useful for parametrization of acoustical models (Chapter 3.5), which again are useful for converting acoustic data from hull-mounted acoustic equipment to abundance

When it comes to converting acoustic data to actual biomasses with accuracy, we are still dependent on physical samples from trawls. For a few species, however, especially *Maurolicus muelleri*, the acoustic modelling is approaching a stage where it may allow accurate biomass estimates based on acoustic data (Chapter 3.4).

Inversion of broadband acoustic data shows promise for biomass estimation (Chapter 3.4), but the method is at an early stage, and dependent on several conditions being met. While optical methods (Chapter 2) show some promise in identifying (and measuring) especially fragile organisms, unknown magnitude of biases introduced by the need to get the optical devices close to the organisms (e.g. avoidance and attraction) make it hard to trust these data for general abundance and biomass estimates.

Physical catches (Chapter 1) are therefore still essential for both taxonomic resolution and biomass estimates, as well as to interpret the acoustic data, even if trawling for mesopelagic organisms comes with its own set of biases and problems.



## Table of Contents

Introduction:.....	6
1. Work, methodologies and developments related to the use of physical catches/trawls/nets in identification and direct mesopelagic biomass estimates .....	9
1.2 Catch equipment design and testing.....	9
1.3 Work on catch equipment monitoring.....	11
2. Work, methodologies and developments related to the use of imaging devices in identification and mesopelagic biomass estimates .....	13
2.1 Implementation of acoustical-optical methods, JUVENA survey activities.....	13
2.2 Identifying siphonophores.....	14
2.3 Cod-end camera systems .....	17
3. Work, methodologies and developments related to the use of acoustic technology in identification and mesopelagic biomass estimates .....	20
3.1 Use of submerged equipment for improved TS estimates .....	20
3.2 Use of acoustic data for scatterer identification .....	22
3.2.1 IMR.....	22
3.2.2 MFRI .....	24
3.2.3. DTU: Separation of fish and siphonophores through combined acoustic and optical measurements:.....	30
3.3 Direct estimates of mesopelagic abundance based on echo counts .....	31
3.4 Improved parametrization of resonant scattering models .....	34
3.4.1 Direct/physical measurements that will improve our ability to parametrize models 34	
3.4.2 Model implementations.....	34
3.4.3 Estimates of model parameters through model inversion.....	38
3.4.4 Inversion of scattering models for biomass estimation .....	40
Conclusion/summary.....	43
References.....	44
Supplementary information: .....	46
Tables.....	46





This project has received funding from the EU  
H2020 research and innovation programme  
under Grant Agreement No 817669



## Introduction:

This report summarizes approaches taken by the different partners in the MEESO project to improve current methods for surveying composition, abundance and biomass of smaller mesopelagic organisms. The project is mainly focused on organisms in the micronekton/macroplankton size range (~2-20 cm), but since we in general have only limited knowledge of behaviour of species in this group, we will consistently call them micronekton, without regard for whether they control their own horizontal distribution by active swimming (as true nekton do). A general document on sampling of mesopelagic micronekton would be too large an undertaking for this report, we have therefore restricted the scope to focus on new or novel methodology used, or projected to be used, by the project partners to survey composition, abundance and biomass of mesopelagic micronekton during MEESO.

There is no such thing as an unbiased biological sampling gear, and to interpret the results of each type of equipment, it is necessary to understand both how that particular gear works, as well as to have a basic understanding of the organisms being sampled. We will start the report by identifying some of the main challenges in surveying mesopelagic micronekton, broken down for different types of gear where natural.

For physical sampling gear (e.g. trawls/nets) the first issue (P1.1<sup>1</sup>) is that the mesopelagic organisms by definition inhabit deep waters (at least during daytime), making it relatively physically challenging to reach their habitat, regardless of type of equipment (Webb et al., 2010). Secondly (P1.2), the organisms in the micronekton size range tend to occur on average at low densities but may occur locally in high densities. This patchiness, with densities spanning orders of magnitude, occurs both in the horizontal dimension (e.g. horizontal gradients and aggregations), but is typically also present in the vertical dimension (e.g. in vertical layers). While the size distribution of mesopelagic fishes must still be considered largely unknown, the fact that many of these fishes can reach weights well above 10 g WW ind<sup>-1</sup> implies that huge volumes must be sampled to get representative numbers for “average” biomass, even if we ignore the uncertainties introduced by the large gradients in densities. To illustrate this point, if the surface integrated sum of all mesopelagic fishes averages 1 g WW m<sup>-2</sup> globally (Lam and Pauly, 2005), this “average biomass” could potentially be made up by a single 10 g mesopelagic fish under a 10 m<sup>2</sup> surface, i.e. a single fish in a volume of ~8000 m<sup>3</sup> (200-1000 m depth range, 10 m<sup>2</sup> area). Thirdly (P1.3), defined as micronekton, most of these organisms are quite mobile, and avoidance of sampling gear has been suggested to be important (FAO 1980, Kaartvedt et al. 2012). This last point probably interacts with the first: our sampling gear constitute a very large disturbance in the otherwise relatively featureless mesopelagic zone, and may be expected to influence the behaviour of organisms found there.

Acoustic equipment has the capacity to efficiently sample very large volumes, and at least for low frequency equipment the two primary challenges to physical sampling gear has little relevance: a low frequency echosounder can sample the entire vertical extent of the mesopelagic zone in a single sound emission, and the sampled volume

---

<sup>1</sup> Problems/issues identified will be enumerated sequentially in the introduction, we will refer to these codes again when describing methods implemented.



is no longer a restricting factor. Studies of mesopelagic distribution therefore often include data from hull-mounted echosounders, often as their primary source of data.

Conventional use of acoustic data is through the “Echo integration” method, where the total backscattered sound over some depth range is summed (integrated), the integrated sound is then converted to abundances by dividing by the average amount of sound scattered by an individual (the so-called target strength or TS). More advanced approaches first divide up the total integrated signal to sub-components, usually aiming to estimate contribution for different groups with very different acoustical properties (for instance swim-bladdered fish vs crustaceans), each of which can then be converted to numerical abundances based on either an average TS or a TS distribution (for instance size based). Methods exist that can be used to directly acoustically measure the size of at least some mesopelagic organisms (e.g. Giorli et al. 2018, Kubilius et al. 2020), but the number of works applying these methods are few. Current acoustic methods for estimating mesopelagic biomass can be viewed as consisting of 2 steps: converting acoustic signals to abundances (S1), and then converting the abundances to biomasses (S2).

There are at least 4 main obstacles that hampers the use of acoustics for estimating mesopelagic biomasses. Firstly (P2.1), there is a general lack of data on the acoustic properties of mesopelagic organisms. For hull-mounted data, this means that even if it is easy to measure the total amount of sound (e.g. often given as Nautical Area Scattering Coefficient, NASC) scattered back from the mesopelagic community, converting the total sound to a total number of organisms present requires assumptions as to how much sound an average organism scatter (target strength, TS). This is related to the second main issue, the identification of the scatterers (P2.2). Since the observation volumes are large, the total backscattered signal is usually the combination of signals from many individuals, and in the deep mesopelagic usually a mixture of taxonomic and scatterer types: finding suitable conversion functions for going from a mixed total acoustic signal to total organismal abundance is obviously non-trivial. The third issue (P2.3) can be seen as a combination of the preceding two: organisms without gas-filled inclusions (e.g. Crustaceans, jellyfish, but also cephalopods, whose main backscatter originates from the beak, as well as fishes without gas-filled swim-bladders) scatter little sound at the lower frequencies needed to cover the mesopelagic zone: as a result they are hard to detect using hull-mounted echosounders, and in practice current acoustic based surveys are likely to be biased towards species with gas-inclusions.

The final main obstacle to obtaining biomasses from acoustic data combines issues with both physical catches and acoustics (P2.4): acoustic backscatter is normally assigned to different taxonomic groups based on contents in net catches (“ground-truthing”), and composition and average weights or lengths used to compute both TS and the final biomass are also typically taken from the catches. If taxonomic and size distributions from the catches are biased, the acoustic analysis is confounded.

Even if methodologies utilized for mesopelagic sampling differs between the partners, work undertaken in the MEESO project has sought to address several of these issues. This report focuses on new methodology developed or utilized as part of the MEESO drive to obtain better identification and estimates of mesopelagic biomass and is a part of a 3-report series from MEESO WP2. It is accompanied by a report focusing on



methods for quantifying biases in the methods used to estimate mesopelagic biomasses. We could organize the report either on a per partner basis, or on a per topic basis. Since many of the methods are similar, or have similar rationales, we opted for the latter, but will, for each type of method, indicate which partners utilize the methodology, and a contact-person at each partner, should more details or actual results be desired. The aim of this report is not to present results obtained with the different work or methodologies, for that either the MEESO data repository or the individual partners should be contacted.





# 1. Work, methodologies and developments related to the use of physical catches/trawls/nets in identification and direct mesopelagic biomass estimates

## 1.2 Catch equipment design and testing

Comparisons of catch equipment and catches

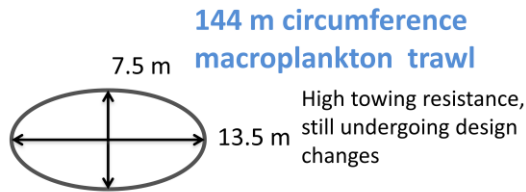
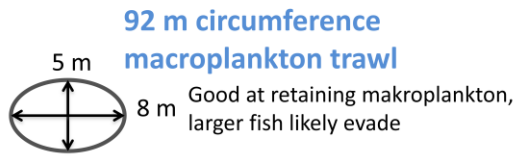
IMR has developed and tested a series of pelagic trawls to capture mesopelagic organisms including fishes, cephalopods, cnidaria and large crustaceans. All these trawls are based on the principle of filtering rather than herding and employ single-size mesh liners from the trawl opening to codend. Strength is provided by large mesh covers. This contrasts with standard pelagic trawls which have graduate mesh sizes, starting with large meshes in the front parts (openings many times greater than the size of most mesopelagic species) which are reduced gradually to sizes too small for the target organisms to escape in the codend. The trawls have been tested in a series of research cruises targeting mesopelagic species in both the open North Atlantic Ocean, Norwegian Sea and fjords on the western coast of Norway.



For the smallest organisms, a trawl with 92 m circumference (distance around the mouth of the belly area, including the wings) and lined with 8 mm (3 mm × 3 mm light opening) knotless mesh was used. The wings have reduced length in order to reduce herding in front of the trawl. In practice, this trawl has an observed opening 5 m high × 8 m wide for a calculated area of 34 m<sup>2</sup> at about 2 knots towing speed. Tests of a scaled-up version of this trawl (144 m circumference, 7.5 m high × 13.5 m wide opening for area of 79 m<sup>2</sup>) showed that towing resistance was too high to be practically usable. The scaled-up trawl has undergone modifications and will be tested again in early 2021.

Two trawls with significantly greater opening area have been tested for larger organisms, which likely possess sufficient swimming capacity to evade the small mouth openings of the trawls described above (P1.2, P1.3). First, a 400 m circumference trawl (opening measured 24 m high × 42 m wide for 792 m<sup>2</sup> opening area) with 7 mm × 7 mm light opening mesh liner was tested. This trawl also proved to have unreasonably high towing resistance (40 tonnes) and was difficult to handle on deck and while setting out and retrieving. A second “large” trawl also with 7 mm × 7 mm light opening mesh liner has proven much more appropriate as a sampling gear for the larger mesopelagic fishes. This trawl has 280 m circumference and an opening measured at 18 m high × 25 m wide for an opening area of 345 m<sup>2</sup>.

Opening mouth geometry and towing resistance for the four trawls tested by IMR is provided in figure 1.2.1, below. More detail on the construction of the two most promising trawls (92 m circumference, 3 mm × 3 mm light opening and 280 m circumference, 7 mm × 7 mm light opening) is shown in Figure 1.2.2.

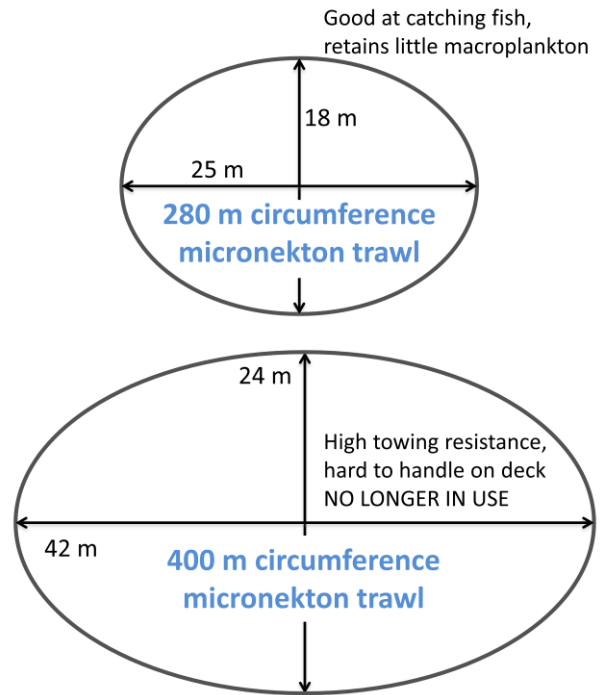




Trawl	Opening area	Mesh size (nominal)	Mesh light opening	Towing resistance
92 m	34 m <sup>2</sup>	8 mm	3x3 mm	14 t
144 m	79 m <sup>2</sup>	8 mm	3x3 mm	22 t
280 m	345 m <sup>2</sup>	16 mm* 	7x7 mm	28 t
400 m	792 m <sup>2</sup>	20 mm* 	7x7 mm	40 t

\* Same 'light opening' due to different twine thickness

Figure 1.2.1. Opening geometry, mesh size (liner), and towing resistance for the four trawls tested by IMR to sample in the mesopelagic zone.



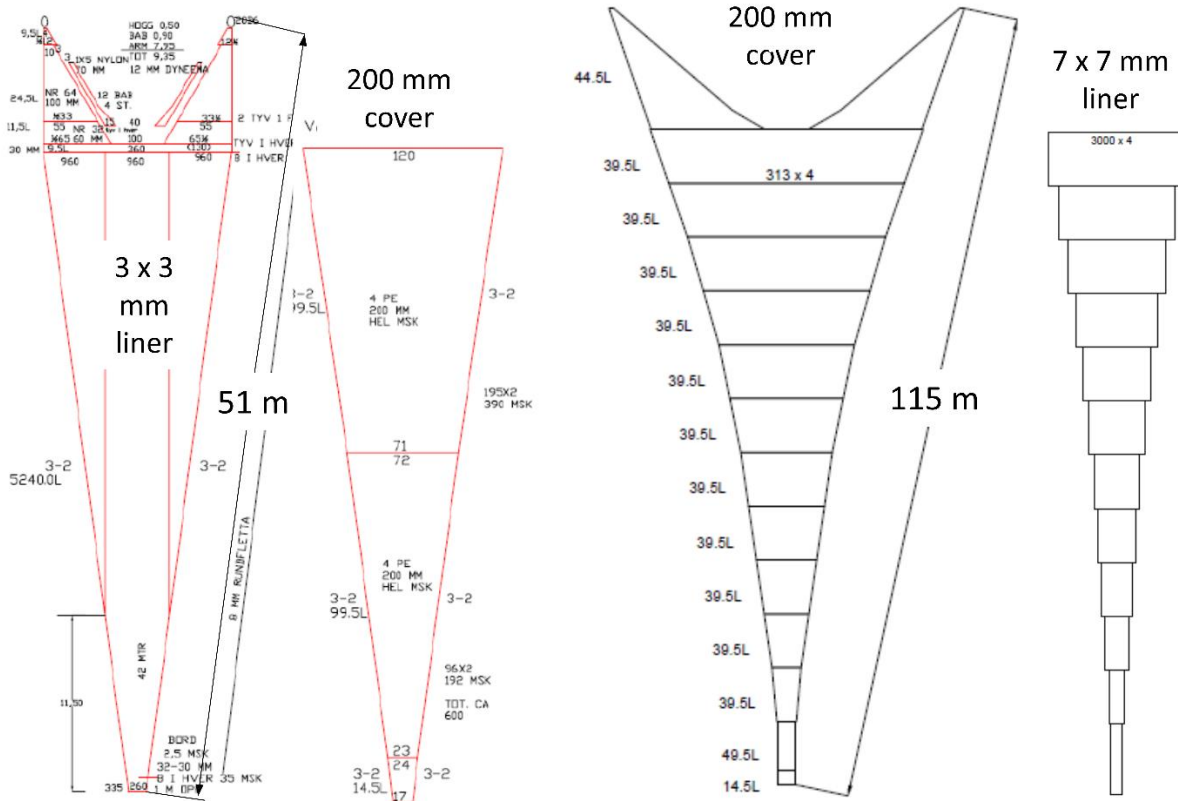
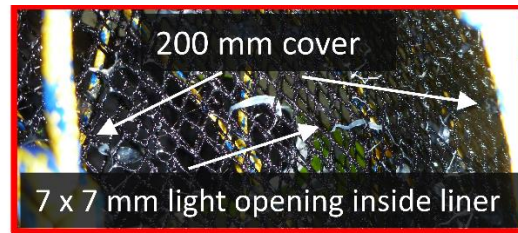
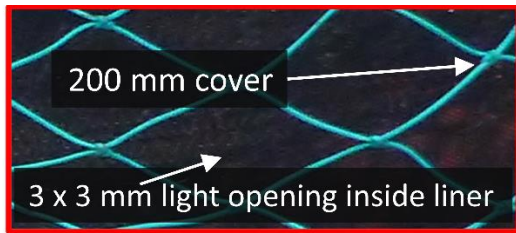


Figure 1.2.2. design of 92 m circumference macroplankton trawl (left) and 180 m circumference micronekton trawl (right). Photographs at top show the cover mesh (green / yellow) and liner mesh (black).

The trawls are fished using very large pelagic trawl doors (12 m<sup>2</sup> Vónin “Tornado”), which generate excessive spreading power for the trawls’ sizes. Overspreading of the trawl is, however, prevented using two constraining ropes between the wing tips, one rope linking the lower wing tips and one linking the upper wing tips. In this way, the trawl doors are kept well outside the path of the trawl (overspread relative to the trawl opening) but the trawl opening width remains constant. The smallest trawl is routinely used with smaller doors (7 m<sup>2</sup>)

### 1.3 Work on catch equipment monitoring

Sampling trawls used to collect mesopelagic organisms are dynamic structures that are constantly changing (e.g., from water currents, towing speed). However, traditional methods to estimate the sample volume (multiplying the theoretical opening area and the total distance covered) does not account for the changes in the trawl geometry while the trawl is towed from 0 – 1000 m depth and back. To account for the changes in the trawl, IMR monitored the trawl’s geometry and water flow at the entrance of the trawl to calculate the average sample volume per minute. Horizontal distance sensors as well as the difference between depth sensors at the entrance of the trawl provided

opening area data while an Acoustic Doppler current profiler (Fig. 1.3.1) provided water flow measurements.

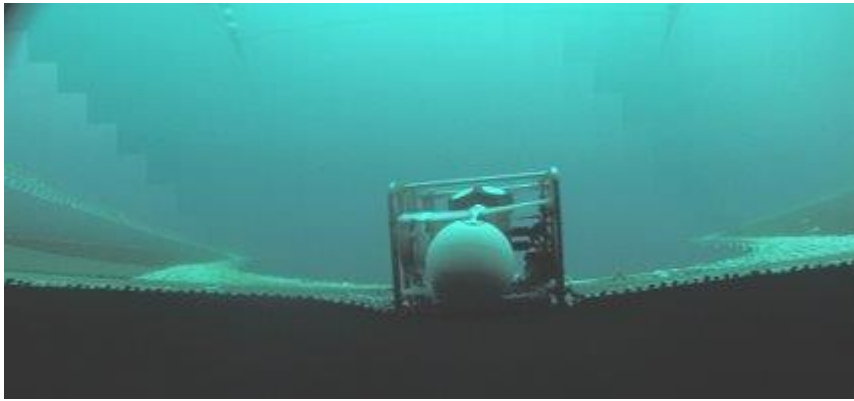


Figure 1.3.1. The Acoustic Doppler current profiler at the trawl entrance during a haul.

## 2. Work, methodologies and developments related to the use of imaging devices in identification and mesopelagic biomass estimates

### 2.1 Implementation of acoustical-optical methods, JUVENA survey activities

In AZTI, the tasks involving implementation of acoustical and optical methods for improved mesopelagic species discrimination have been conducted mainly during the JUVENA survey. JUVENA is primarily a trawl acoustic survey devoted to estimate abundance and spatial distribution of small pelagic species in the Bay of Biscay, with particular focus on European anchovy (Boyra *et al.*, 2013). Two surveys have taken place since the beginning of MEESO project, the first one conducted between the 1<sup>st</sup> and 30<sup>th</sup> September 2019 and the second one from 17<sup>th</sup> August to 30<sup>th</sup> September 2020.

The methodology of the survey was adapted to include different tasks involving improved sampling of mesopelagic species. In this sense, although the recording of acoustic data on transects was done in narrowband multifrequency acoustic mode, at 18, 38, 70, 120 and 200 kHz frequencies, frequency-modulated multiband acoustic data was recorded during the trawls, at 38, 70, 120 and 200 kHz central frequencies.

In each survey, over 20 trawls were done directly at the mesopelagic layers (from 75 to 500 m depth). In these trawls, practically the only mesopelagic species captured was *Maurollicus muelleri*. Positive trawls on mesopelagic species were used to identify suitable areas of testing and implementation of new sampling methods.

In addition, 20 fixed WBAT (at 70 and 120 kHz frequencies) stations were done on the Rosette or standalone (Table 2.1, Figure 2.1.1) focusing on verified *M. muelleri* aggregations during vertical migration. The main objective of the WBAT recordings is studying the impact of swimbladder adaptation to depth changes on the TS-length relationship of this mesopelagic species. The WBAT was calibrated in each survey both at the surface and at the typical depths of the mesopelagic recordings, prior or after the survey.

Finally, in JUVENA 2020 took place the first tests of WBAT installed at the headrope of the pelagic trawl (Figure 2.1.1). These experimental hauls were successful in setting up the maneuver and providing valid acoustic recordings of the fish entering the net, but unfortunately, we were not successful in catching *M. muelleri* at these trawls. Contact person: Guillermo Boyra (gboyra@azti.es).





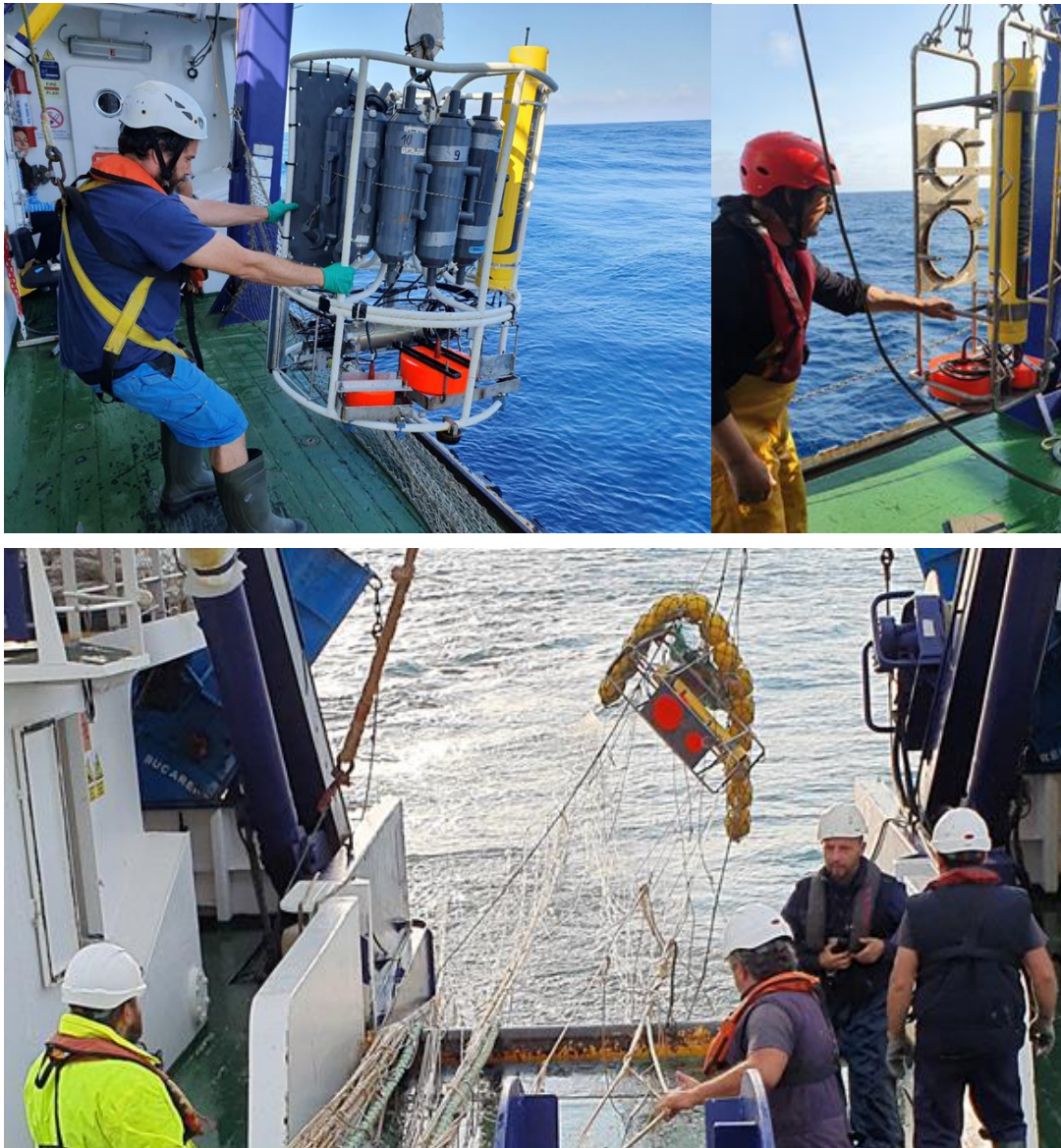


Figure 2.1.1. Illustration of two vertical WBAT stations (top), in the Rosette and standalone, and the preliminary tests of WBAT at the headrope of the pelagic trawl during JUVENA 2020 (bottom).

## 2.2 Identifying siphonophores

DTU is currently using data obtained with a stereo-camera system in combination with broadband acoustic data to separate physonect siphonophores and mesopelagic fish.

DTU has used a lowered acoustic probe (Fig.2.2.1 ) equipped with split aperture broadband echosounders (35-45, 55-90 and 160-260 kHz, and a stereo camera (two 12.1 Mpx Imenco SDS 1210 underwater photo cameras) to study the mesopelagic layer at close range. Physonect siphonophores were observed by the stereo camera throughout the water column (Fig.2.2.1), while sightings of mesopelagic fish were more rare due to avoidance (Fig.2.2.1).

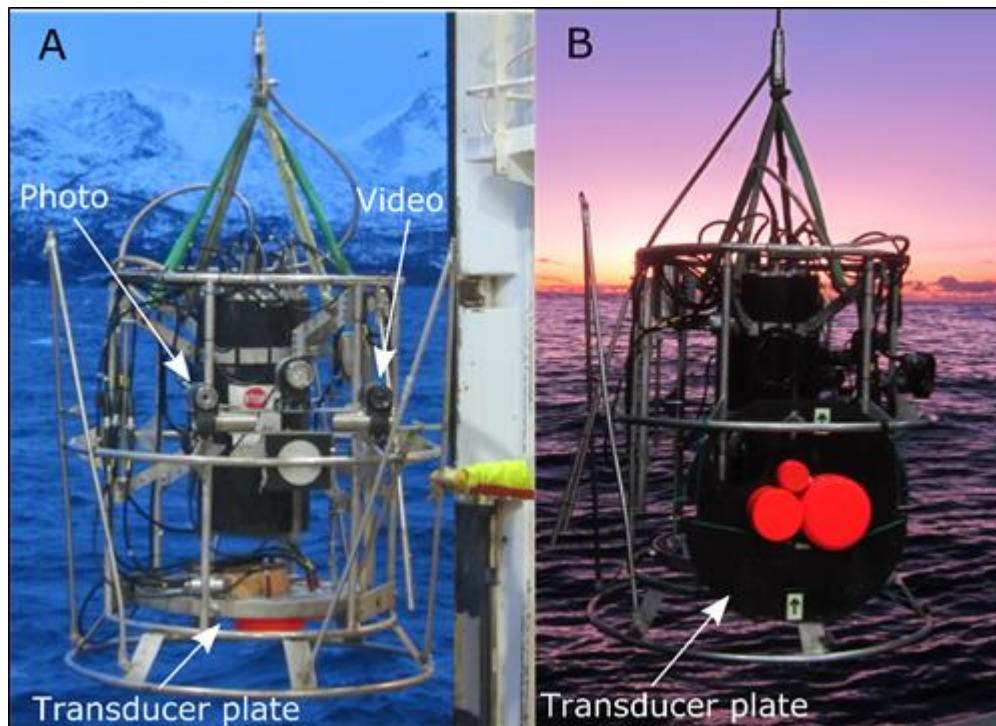


Figure 2.2.1 Above: TS-probe used mounted with broad band split beam aperture and stereo camera. Below: Image identification of physonect siphonophore *Nanomia cara* at 75 meters and mesopelagic fish *Benthoosema glaciale* at 450 meters.

IMR has experimented with putting cheap camera systems (e.g. GoPro) on CTDs to evaluate the use of simple, cheap systems for registering the presence/absence of siphonophores. While other data (see below) suggested that siphonophores were rare at that station, the GoPro shutter speeds were not sufficient to prevent image “smearing” at the light levels (continuous light) and descent/ascent speeds of the CTD package. It was rapidly concluded that a flash-based system/higher shutter speeds were needed to properly “freeze” the images enough to allow identification of siphonophores. Presence/absence of siphonophores for that cruise was therefore evaluated through a combination of imagery from the Deep Vision trawl camera system (see 2.3 below), and images from a VPR (Video Plankton Recorder) deployed on the MESSOR.



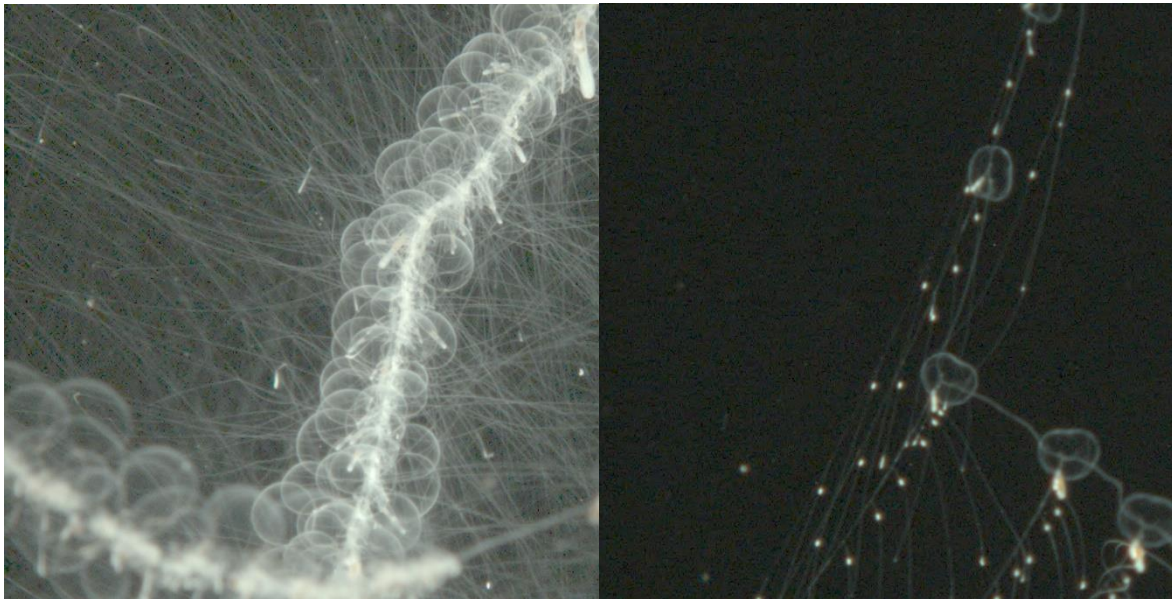


Fig. 2.2.2: Potential siphonophore body parts and feeding nets from VPR images

The VPR imaging volume is very small, but since many siphonophores have extended feeding nets, the probabilities of observing single colonies are much higher than that suggested by the colony density alone, since the cross-sectional area is large (e.g. Robison et al. 2020, Fig. 2.2.2). The Deep Vision has a much larger imaging area, and if the siphonophores do not get entangled in the net ahead of the imager (Fig. 2.2.3), the effective sampling volume depends on the size of the trawl. We treat both VPR and Deep Vision as non-quantitative for siphonophores since the effective sample volumes cannot be estimated, but both instruments should be able to indicate when physonect/cystonect siphonophores occur in densities high enough to present problems for mesopelagic fish identification. Data from the VPR has additionally previously been used to estimate pneumatophore sizes for high densities of larval siphonophores (Benfield et al., 2003).



Fig. 2.2.3: Likely siphonophore seen with the Deep Vision stereo camera system, ~500 m depth (courtesy Mette Agersted, Melanie Underwood, Shale Rosen)



## 2.3 Cod-end camera systems

The Institute of Marine Research has used the Deep Vision trawl camera system (Rosen et al., 2013 and Rosen and Holst, 2013) to image fish as they pass through the extension of the trawl and into the cod-end (Figure 2.3.1). The Deep Vision system collects 5 or 10 sets of stereo images per second. The images are time- and depth-referenced so that the position where each organism passed through the camera chamber can be estimated. An example is provided in Figure 2.3.2, where species assemblage changes from a mixture of mesopelagic fishes, krill and shrimps to exclusively krill and shrimps between 203 and 258 m depth.

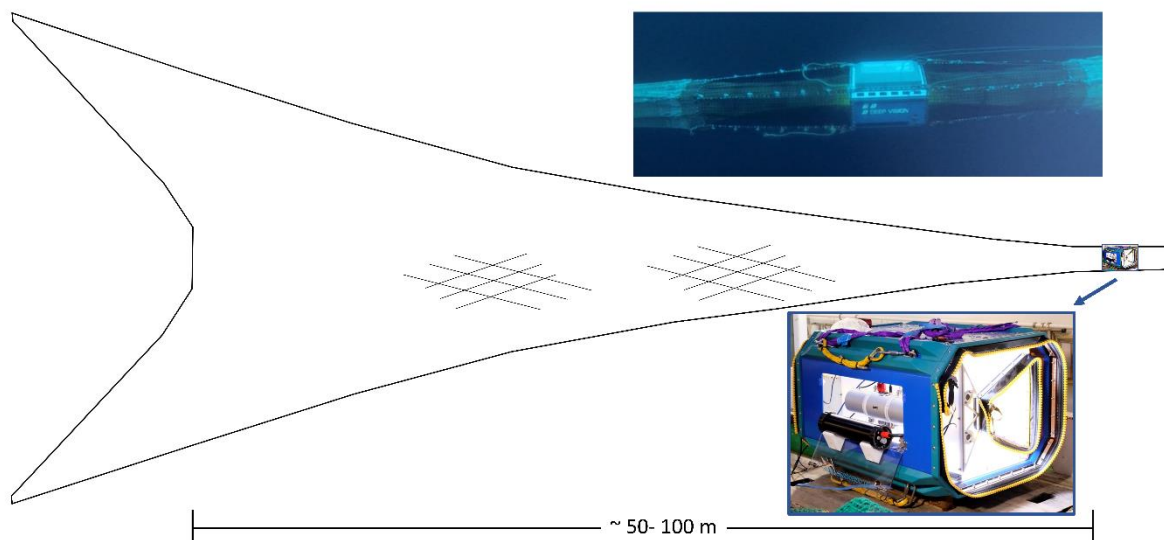
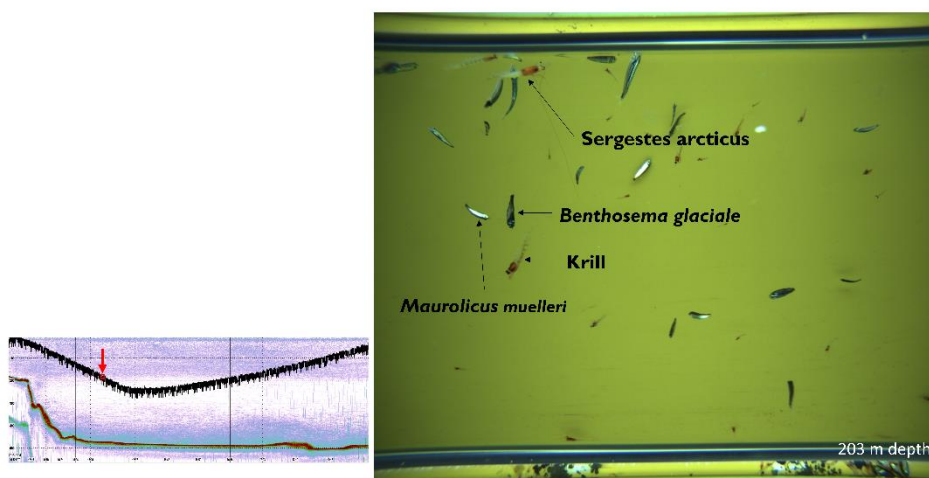


Figure 2.3.1. The Deep Vision camera system is contained in a frame placed between the extension and codend of a trawl.



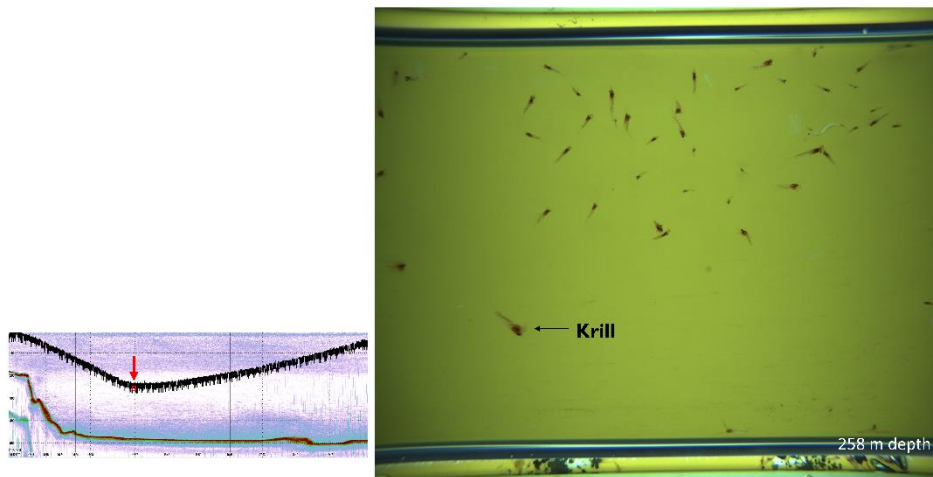


Figure 2.3.2. Example Deep Vision images from an oblique trawl haul to 250 m. Upper image from 203 m depth, lower image from 258 m depth. Echograms at left show backscatter at 38 kHz. Trawl path is indicated in black (unfiltered depth data), position of each Deep Vision image indicated by red arrow and box.

Several modifications have been made to the Deep Vision system to better suit investigations of mesopelagic species. In 2020 the system was run at higher resolution (2456 × 2054 pixels) and red lights were used to reduce the likelihood that the artificial lights would affect behaviour of organisms in the opening of the trawl. In addition, the overall size of the passage where passing organisms are imaged was reduced to ensure they pass closer to the camera for enhanced resolution (Figure 2.3.4).

2018-2019: 1228 x 1027 pixels, white light

2020: 2456 x 2054 pixels, shorter range to fish, red light

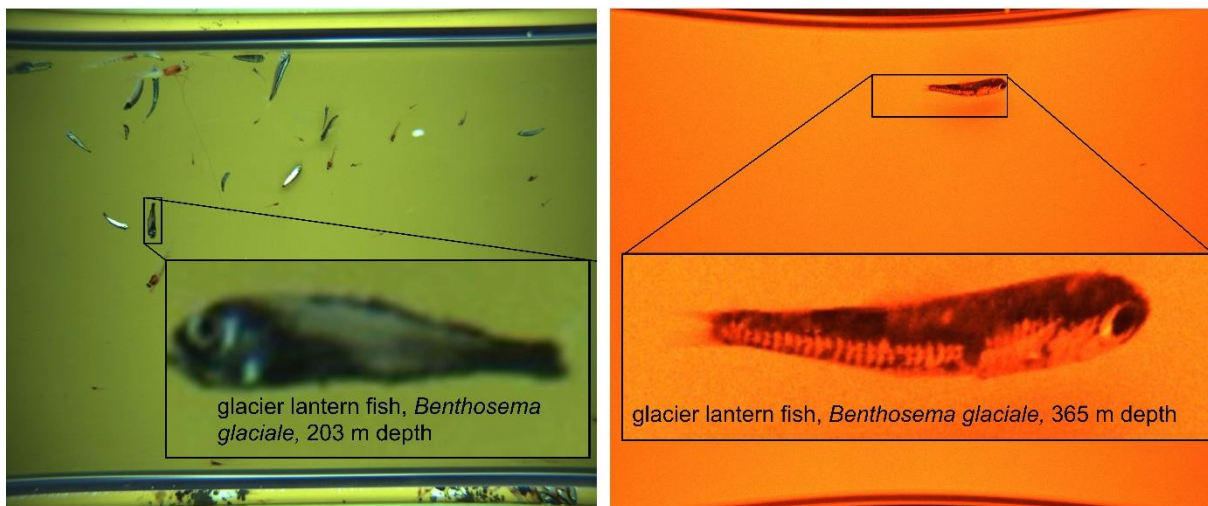


Figure 2.3.4. Example images of *Benthosema glaciale* taken at 1228 × 1027 pixels and white light (left) and at higher resolution of 2456 × 2054 pixels and red light (right).

In addition, the spectrum of light emitted by the Deep Vision system's lights was measured in air and modelled using attenuation coefficients from Moser (1992). Measured spectrum intensity is shown in Figure 2.3.5 and modelled intensity of unfiltered (white) light at ranges of 100 m (distance to the opening of the large trawls) and 50 m (distance to the opening of the 92 m circumference trawl) ahead of the Deep

Vision system in seawater is shown in Figure 2.3.6. The wavelengths of light reaching these distances is higher than the peak spectral sensitivities for *Maurolicus muelleri* (de Busserolles et al, 2017) and Myctophidae family fishes (Douglas and Partridge, 1997).

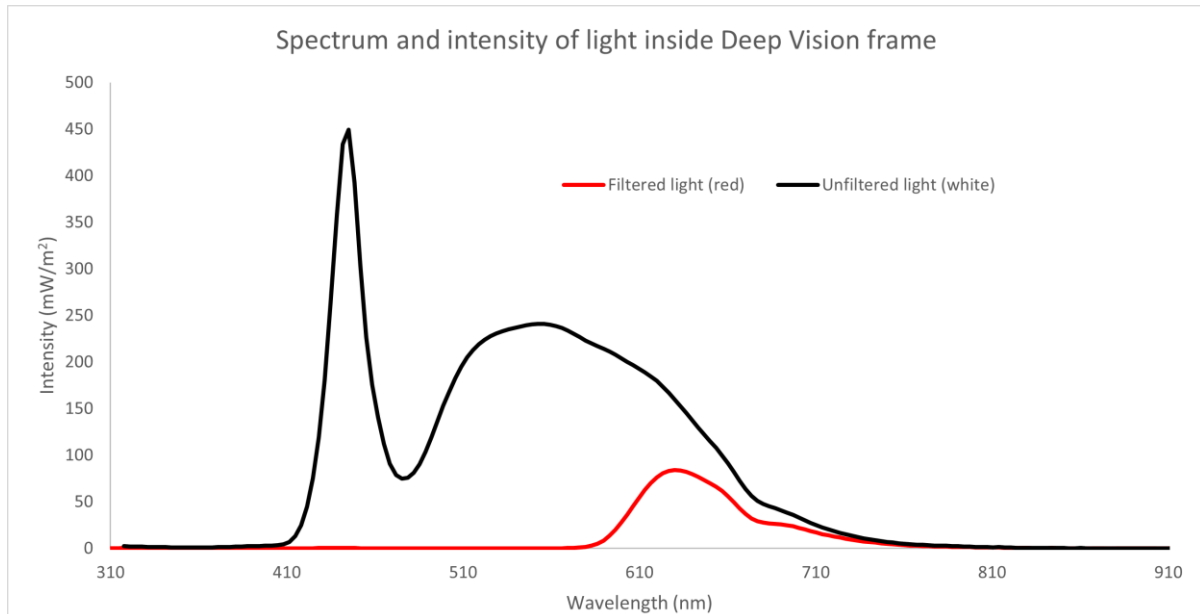


Figure 2.3.5. Measured wavelength and intensity of light inside the Deep Vision system, both with unfiltered (white) lights and filtered (red) lights.

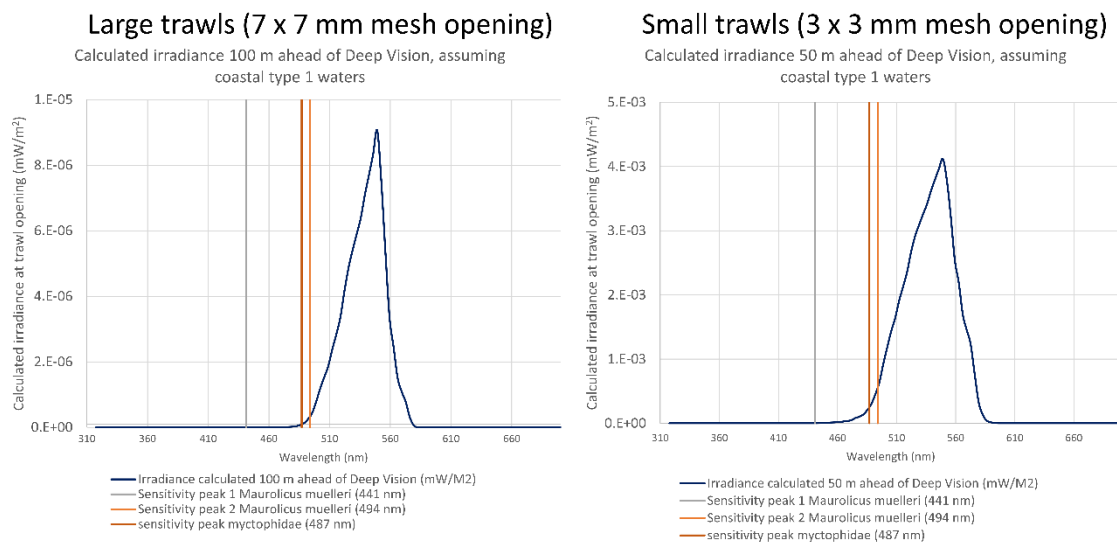


Figure 2.3.6. Modelled irradiance of light (unfiltered white lamps) at 100 m (left) and 50 m (right) distance from the Deep Vision system. Sensitivity peaks for *Maurolicus muelleri* and Myctophidae mesopelagic species are indicated.

### **3. Work, methodologies and developments related to the use of acoustic technology in identification and mesopelagic biomass estimates**

Most of the partners have deployed acoustic devices to mesopelagic depths. The primary advantage of deploying equipment to mesopelagic depths is that it enables measurements on individual organisms; as acoustic equipment utilized by the partners transmit and receive sound in a narrow cone, the observed volume is directly related to the range between the observation and the transducer. Individual targets can only be resolved if there is one or fewer target per ensonified volume, the ensonified volume is the product of the (range-dependent) area covered by the acoustic beam, and the effective pulse-length of the transmission. Since broad-band acoustic echosounders can achieve much shorter effective pulse-lengths than narrow-band equipment, the use of broad-band equipment optimizes the possibility of resolving individual scatterers. A secondary benefit of submerging acoustic equipment is that it enables measurement at higher frequencies in the mesopelagic zone: seawater absorbs acoustic energy quicker at higher frequencies, and this absorption limits the effective observational range of echosounders, in practice a 120 kHz hull-mounted echosounder can just observe the upper ranges of the mesopelagic. The advantage of also obtaining data at higher frequencies lies primarily in that it enables observation of organisms that scatter little sound at the lower frequencies (e.g. euphausiids, salps and other “weak” and smaller scatterers, P2.3), secondarily in that the increased information may allow improved inferences about acoustic properties (P2.1) of targets also observed at the lower frequencies, this increased information may therefore be useful for identification of the scatterers (P2.2).

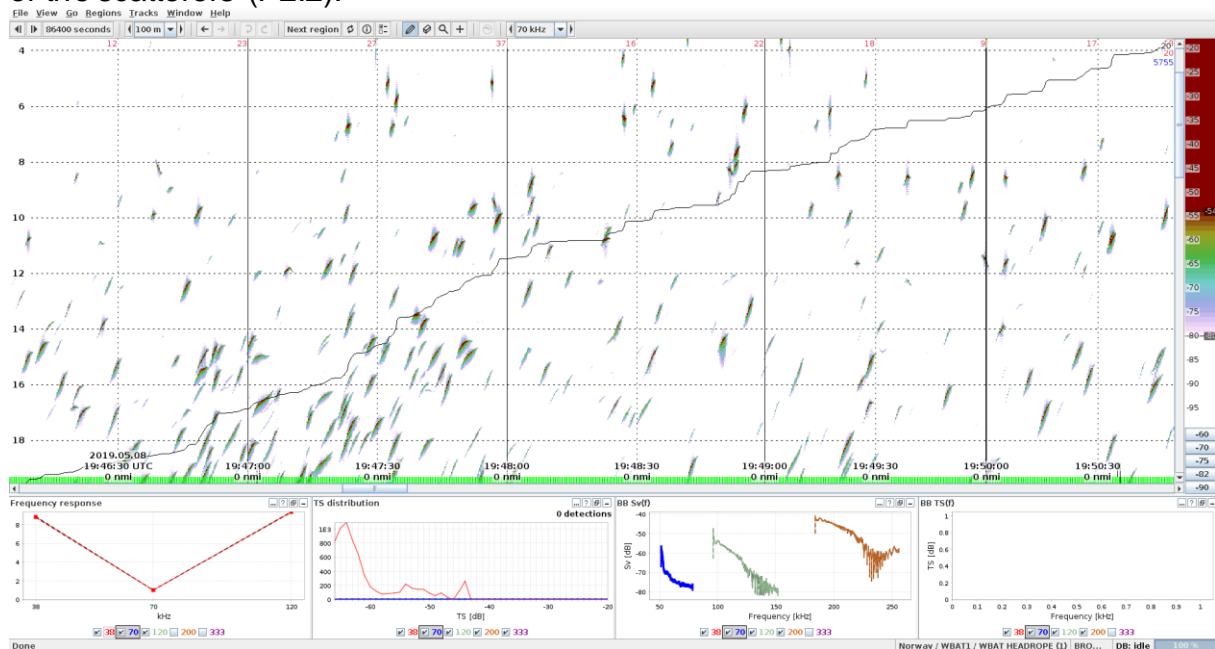


Fig. 3.1: High resolution echogram showing echoes from resolvable individual organisms inside a scattering layer, 70 kHz FM from towed body “MESSOR” (Data source: IMR).

#### **3.1 Use of submerged equipment for improved TS estimates**

When the frequency and orientation (e.g. vertical sound emission) of the submerged equipment matches frequencies and orientation of the hull-mounted equipment, the

submerged equipment may give direct estimates of *in situ* target strength (TS) and can be used to address S1 and P2.1.

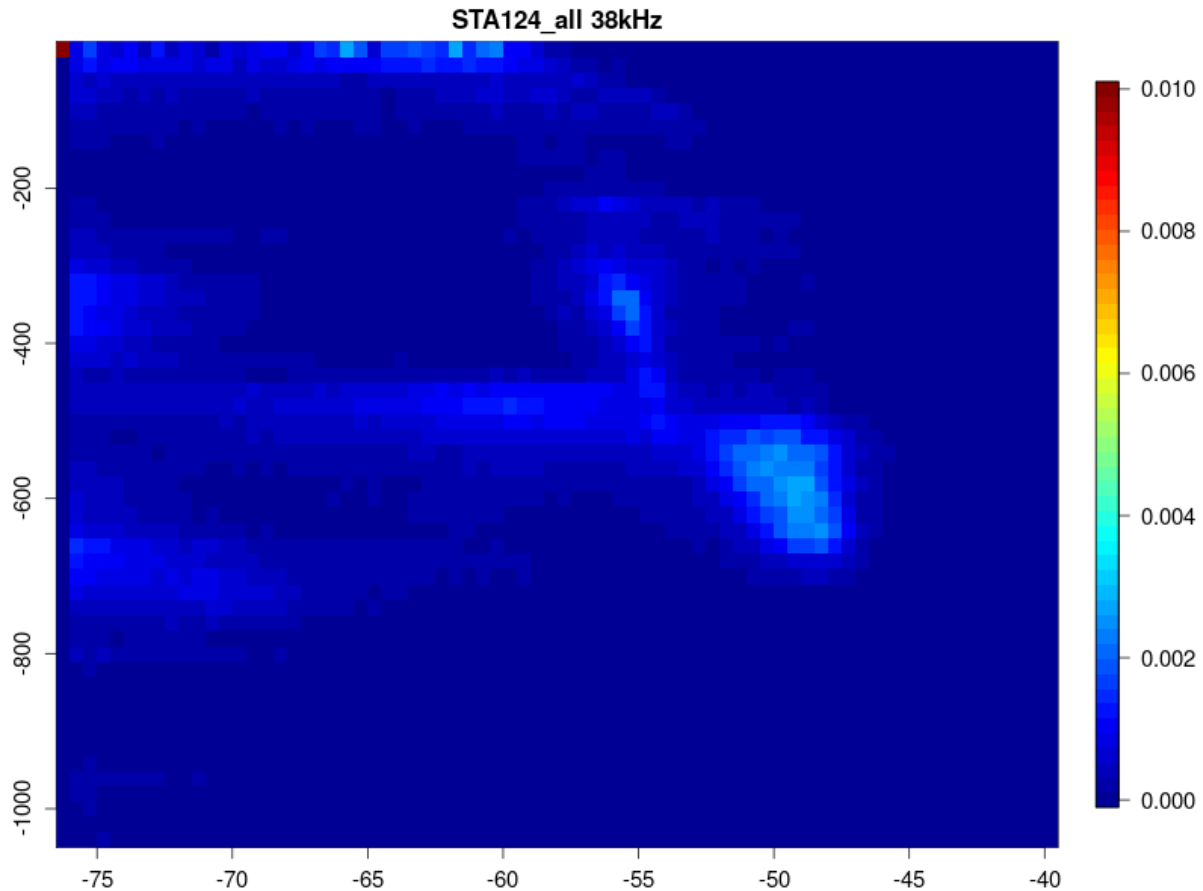


Fig. 3.1.1: The figure shows densities of detected *in situ* echoes (vertically oriented 38 kHz transducer, CW mode) plotted against depth and target strength (TS, dB), from a single station during the 2019 G.O. Sars cruise from Cape Verde to Norway. Depth resolved average TS values can be easily computed from these data and can be directly used instead of modelled TS values in converting integrated backscatter to organismal densities.

IMR has during cruises aimed at studying the mesopelagic, routinely collected vertically oriented echosounder data from a towed body, down to a depth of ~1000 m. Due to the high availability of submerged acoustic equipment during specialized mesopelagic cruises, IMR has however opted not to use echo integration for acoustic abundance estimations during these cruises (S1, see Direct estimates of mesopelagic abundance based on echo counts below). The only place IMR currently use hull-mounted echosounder data for estimation of mesopelagic biomasses in MEESO is in the estimation of biomass of *Maurolicus muelleri*, but in general this species often occurs in high enough local densities that single organism echoes during daytime are not obtainable. While our results for TS at depth (38 kHz CW, 70 kHz FM, 120 kHz FM, 200 kHz FM) will be used for other purposes, they will not be used directly to scale hull-mounted results, since we in general do not use the hull mounted data for mesopelagic biomass estimation. Contact person: Thor Klevjer (thor.klevjer@hi.no)



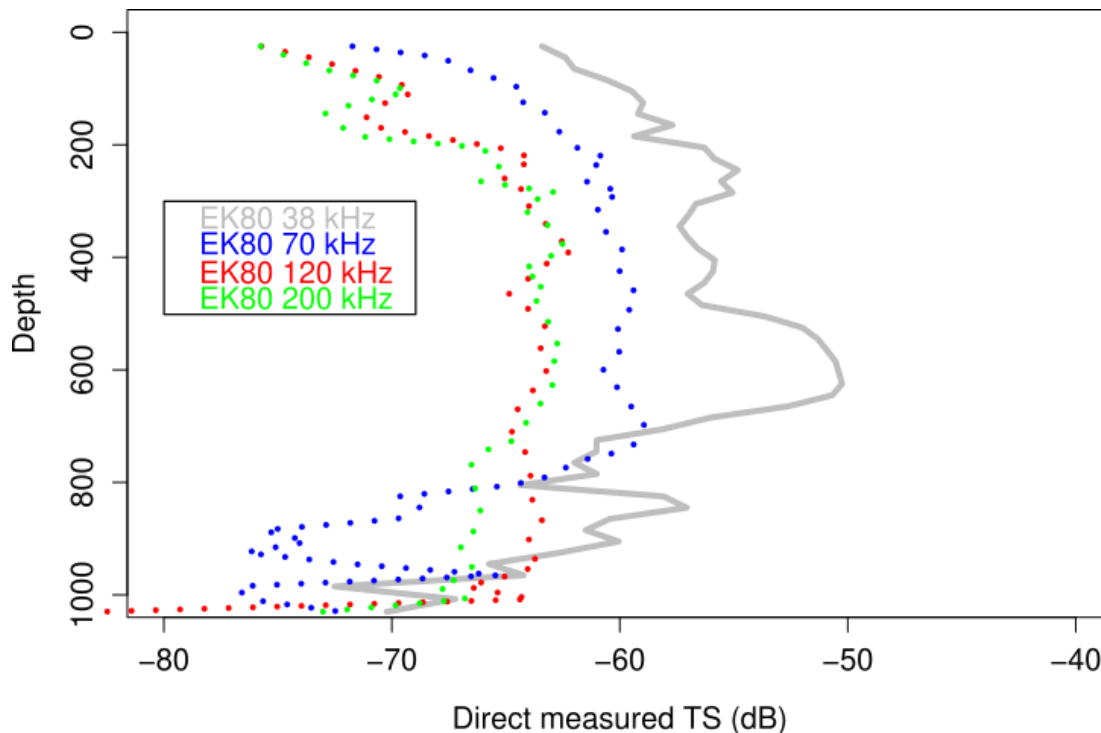


Figure 3.1.2: Average TS (dB) against depth, for 4 different frequencies, based on direct measurements with the split-beam method, on data from acoustic equipment deployed on the towed body, same station as Fig. 3.1.

## 3.2 Use of acoustic data for scatterer identification

### 3.2.1 IMR

In addition to being directly relevant to conversion of integrated acoustic signals to abundances (S1) through the information on acoustic properties (P2.1), the TS measurements at depth can potentially also be used in identification of scatterers (P2.2/2.3), at least to coarse acoustic categories. Similar methods have previously been used to group volume backscattering data (for instance Korneliussen *et al.* 2016 for a practical example of how such functionality can be incorporated in software). In the case of classification of single echo acoustic signatures interpretation is simplified by not having to consider signals from mixed assemblages. Theoretical scattering models exist that can potentially be adapted for mesopelagic organisms, once appropriate values for model parameters are determined (see chapter on Scattering models below), but even without detailed parametrisations comparison of expected frequency spectra from models with observed spectra can be used for a coarse alignment between acoustically identified categories and organism types. A primary concern in the scientific literature is about the perceived importance of resonance of air-inclusions for biomass estimates obtained at 38 kHz (P2.1/2.2, e.g. Davison *et al.* 2015, Proud *et al.* 2019); data identifying densities/proportions of different types of scatterers at depth can be used to directly address these issues.

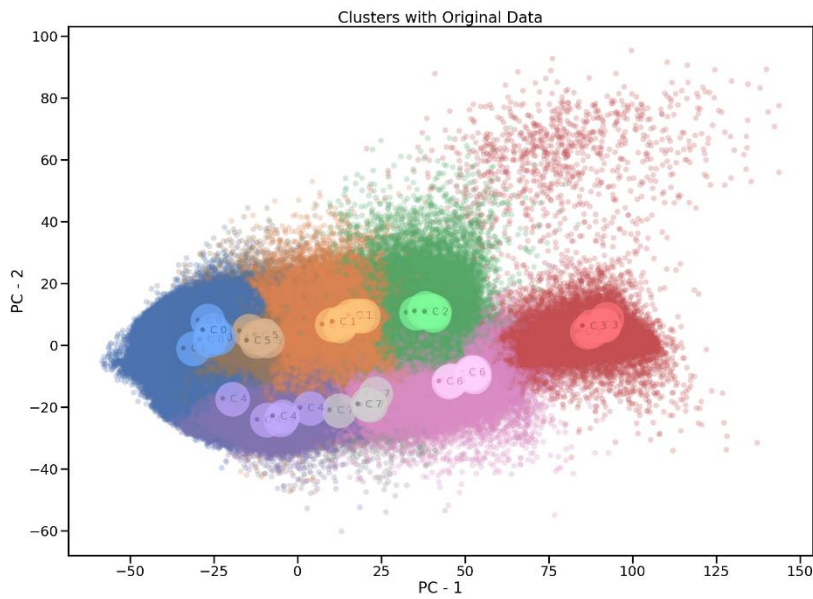


Fig. 3.2.1 PCA plot of clustering results of 70 kHz (FM) single echo data, all recorded echoes from MESSOR deployments during cruise 2019703 (within 3 dB beam width, for ranges 5 to 20 m). Due to large memory requirements, the clustering process had to be split into 6 separate runs (data split at random), the centroids (large blobs) for each run therefore moves a little bit in PCA space between runs.

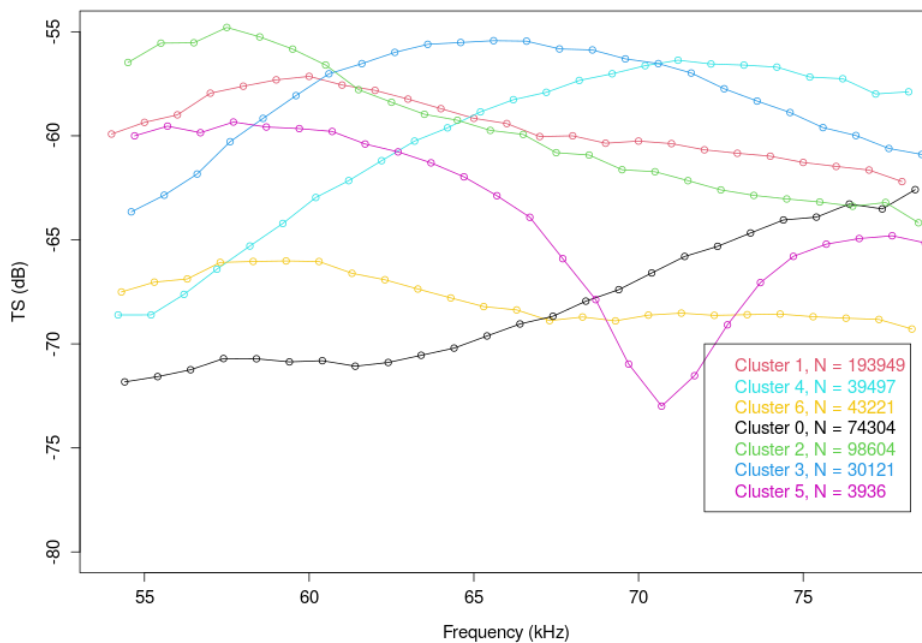


Fig. 3.2.2: Average TS per cluster plotted against frequency for a clustering run with unique clusters, otherwise same data as in the last figure. Note that colours for the different clusters are not corresponding to the colours in the previous figure.

IMR has during mesopelagic cruises prioritised collecting acoustic data from resolved organisms, these data are our primary data-source for acoustic abundance estimates



(S1) during these cruises. Work is underway to utilize these data for mapping of proportions of total scattering at different frequencies to different acoustic categories. Contact person: Thor Klevjer ([thor.klevjer@hi.no](mailto:thor.klevjer@hi.no))

### 3.2.2 MFRI

MFRI main goal within WP2 of the MEESO project is to identify and provide broadband acoustic measurements of deep scattering mesopelagic layers (DSML) to optimise the identification and biomass estimation of mesopelagic organisms.

Mesopelagic layers are composed of a diversity of macrozooplankton and fish species and accurate estimation of the mesopelagic organisms' biomass is limited when using only hull-mounted narrowband echosounders (e.g. Bassett et al., 2020). Several mesopelagic organisms have been observed to have weak backscatter although some species have resonant backscatter properties with variable relation to acoustic frequency and pressure (e.g. Proud et al., 2019). Accurate target strength (TS) is indispensable for precise conversion of acoustic backscatter volume strength to density. Physical features of fish or organisms, such as tilt, size and swimbladder volume and shape, can affect the TS and consequently the estimation of their abundance. However, ground-truth trawl samples provided information that these DSML are composed of several macrozooplankton and fish species, which makes TS estimation challenging. To conduct an accurate estimation of target strength measurements, one therefore needs to compare *in situ* measurement of single echoes of organisms using a submersible echosounder at short ranges to overcome signal to noise ratio limitations and short ranges of higher frequencies in multifrequency and broadband analysis and validate these estimates with the catch or optical instruments and even with theoretical TS model estimates.

For this purpose, the MFRI specifically aims to facilitate the identification of the macrozooplankton and nekton backscatter within DSML and to provide accurate broadband acoustic measurements of these mesopelagic organisms. Results will be compared with recordings made with hull-mounted acoustic system, alongside ground-truth trawl samples of macrozooplankton and nekton collected at these layers.

MFRI sampling for WP2 (and WP4) within the MEESO project took place on the RV Árni Friðriksson during the latter part of the International Ecosystem Summer Survey in Nordic Seas (IESSNS). The second part of the cruise covered sea areas south of Iceland, the Iceland basin and the Irminger basin (13-30 July 2020). Two days were allocated to sampling for the MEESO project, which included four stations taken using several instruments, such a CTD, plankton nets, a pelagic trawl, Video Plankton Recorder (VPR) and a submersible echosounder (Figure 3.2.3).







Figure 3.2.3: Images of some of the instruments used to sample backscatter and macrozooplankton and nekton for the MEESO project. WBT-TUBE submersible echosounder (left image and lower middle image), pelagic trawl being deployed (upper middle image) and retrieving trawl and main catch (right images). Photos by Svanhildur Egilsdóttir.

At the MEESO stations, physical properties of the water column were collected down to 1000 m with a rosette equipped with a Conductivity Temperature and Depth sensors (CTD) and a fluorometer. Water samples were taken at several depths to obtain a profile of chlorophyll and nutrients. Additionally, zooplankton samples were collected using a WP2 net (200  $\mu\text{m}$  mesh size) at two depths (50 and 200 m) towed with a speed of  $\sim 45 \text{ m min}^{-1}$ .

To profile the distribution of plankton within these mesopelagic layers, a VPR was deployed vertically down to 800 m at all MEESO stations (Figure 3.2.4) collecting environmental, fluorescence data and plankton/particles images, taken at a rate of 15 frames  $\text{s}^{-1}$ . Alongside ground-truth trawl samples of macrozooplankton and nekton were collected at these DSML with a pelagic trawl (opening  $\sim 27 \text{ m}^2$ , mesh size 4 mm and 6 mm stretched). At each MEESO station the pelagic trawl deployment focused on two DSML observed in the 18 and 38 kHz hull-mounted acoustics (Figure 3.2.5) and in addition an integrated trawl was deployed down to 1000 m (see WP4 for more details).

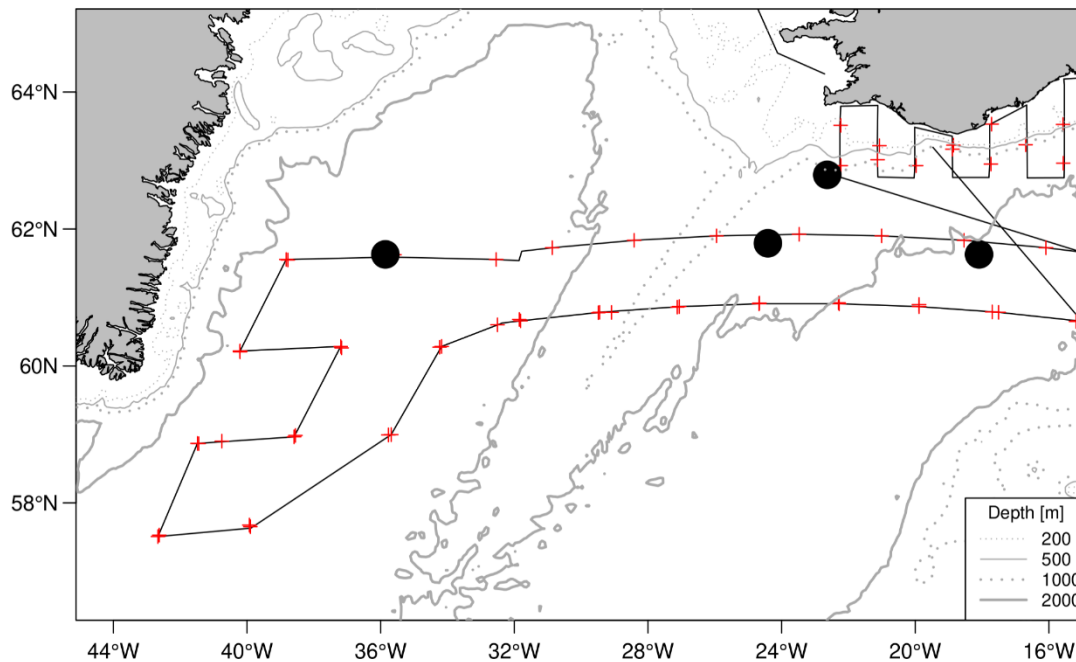


Figure 3.2.4: Map showing the cruise track (black line), IESSNS stations (red crosses) and the position of the MEESSO stations (black dots).

Hull-mounted acoustics data were collected with a calibrated Simrad EK80 echosounder split beam at five frequencies (18, 38, 70, 120, and 200 kHz) at 1 ms pulse duration. Between stations the data were sampled down to 750 m using narrowband. On each MEESSO station, acoustic backscatter was sampled down to 1000 m depth collecting broadband data centred at the frequencies 38, 70, and 120 kHz. Multi-frequency post-processing analysis was performed on the acoustic data with the LSSS (Large Scale Survey System) software (version 2.9.0). Acoustic layers were scrutinized to groups/species level based on each species frequency response and catch composition of the pelagic trawl. Acoustic backscatter was identified to the following categories: Jellies, Red fish, Herring, Krill, Plankton, Squid, Mesopelagic fish & crustaceans, Mesopelagic fish and Other. The defined categories and total backscatter at all frequencies was stored as Nautical Area Scattering Coefficient Values (NASC,  $S_A$ ,  $m^2 \text{ nmi}^{-2}$ ) with -82 dB lower threshold in 0.1 nmi resolution and 10 m vertical resolution.

In the past year, MFRI contribution to WP2 MEESSO project is the development methods of deployment of a submersible echosounder to study and map the mesopelagic organisms at depths observed initially in the 18 and 38 kHz hull-mounted acoustics (Figure 3.2.5).

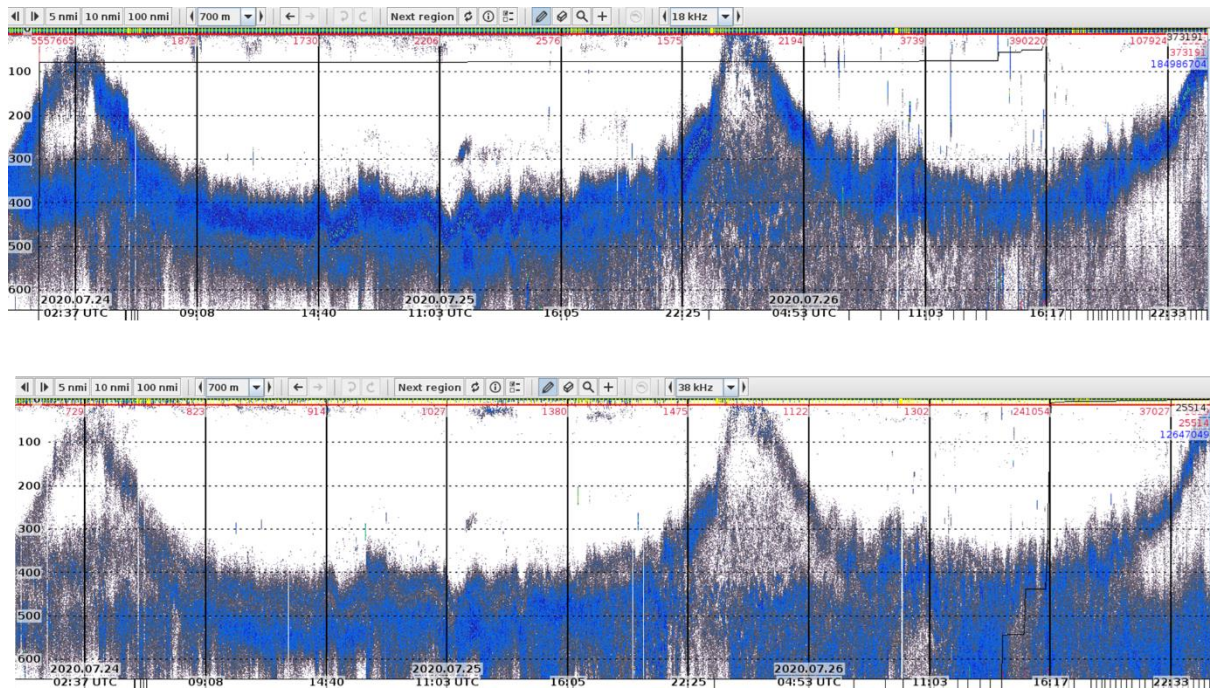


Figure 3.2.5: Example of two days of acoustic backscatter (18 and 38kHz) collected along the uppermost transect ca. 61°50'N (see figure 3.2.4).

The submersible echosounder is equipped with a wide-band echosounder (WBT-TUBE, Simrad EK80, Figure 3.2.3) and ES38 18-DK-split and ES120-7CD kHz transducers and a depth, tilt and temperature sensors. It was first deployed in close proximity of DSML (300 – 500 m) during the IESSNS 2020. The equipment was lowered down to ~50 m distance from each dense DSML (Table 3.1) situated south of Iceland, in the Irminger basin and the Iceland basin. Broadband acoustic data (35 to 45 and 90 to 170 kHz, respectively) were recorded for at least 15 minutes. Backscatter from all targets was stored as Volume backscattering coefficient ( $S_v$ , dB) and Nautical Area Scattering Coefficient Values (NASC,  $S_A$ ,  $m^2 \text{ nmi}^{-2}$ ) with -82 dB lower threshold in 1s analysis windows at ranges of 15-80 m from the transducers.

The submersible echosounder was calibrated both for narrowband and broadband pulses (April 2020) using a tungsten sphere with a diameter of 34.9 mm suspended about 20 m below the submersible transducers. A calibration of the submersible echosounder at different depths was tried in 2020 during two other surveys (International Ecosystem survey in the Nordic Seas and the Autumn Capelin survey, respectively) but due to logistic and weather problems the at-depth calibration was not conducted. A calibration at different depths is planned for the summer of 2021. MFR1 plans to complement to the submersible echosounder with an infrared camera (essential to Task 2.2 in WP2) to better corroborate the organism in each backscatter layer and add a CTD.

### Preliminary findings

Macrozooplankton and nekton were collected at two main DSML evident in the 18 kHz and 38 kHz echograms (Figure 3.2.5). It was clear during the survey that one mesopelagic layer with stronger backscatter at 18 kHz was composed mainly of mesopelagic fish that would conduct a vertical migration at night and maintain a depth of ~300-400 m during the day. Another layer with minimal diel vertical movement with stronger backscatter at 38 kHz between 500-700 m was mainly composed of

mesopelagic fish and crustaceans. Along the uppermost transverse transect the strong acoustic backscatter at 38 kHz was mainly correlated with the appearance of the mesopelagic fishes and crustaceans (Figure 3.2.6).

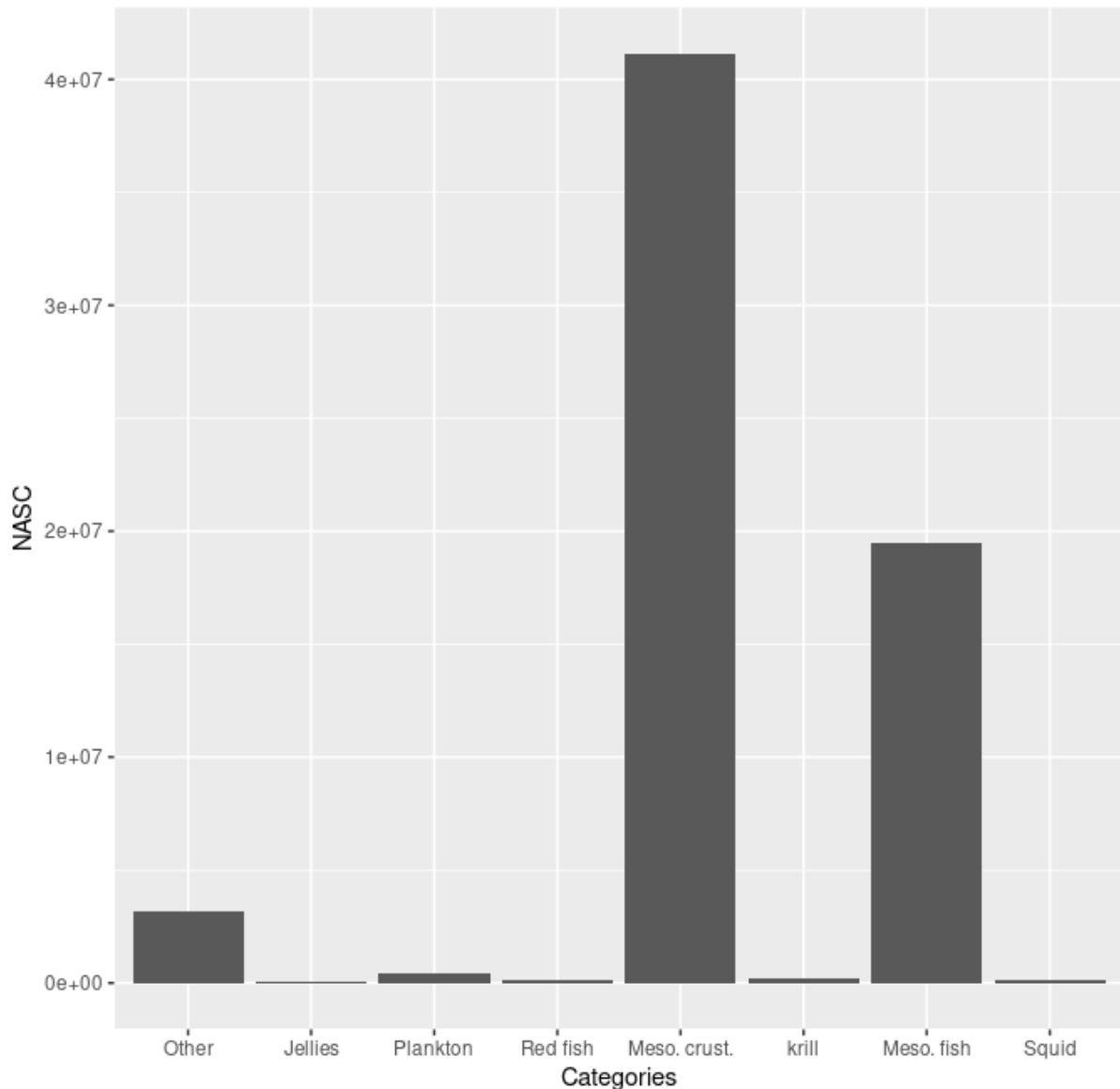


Figure 3.2.6: Total acoustic backscatter (SA values  $\text{m}^2 \text{nm}^{-2}$ ) at 38 kHz for each category scrutinized along the uppermost transect ca.  $61^{\circ}50'N$ . Categories are Jellies, Red fish, Krill, Plankton, Squid, Mesopelagic fish & crustaceans (Meso.crust.), Mesopelagic fish (Meso.fish) and other organisms (Other).

Preliminary results from the submersible echosounder indicate e.g. that backscatter at 120 kHz (Figure 3.2.7) was stronger in the uppermost mesopelagic layer (350 m) than in the lower mesopelagic layer (450 m). Macrozooplankton and nekton tend to migrate to upper layers during the night to feed (Mauchline, 1980; Kaartvedt, 2010), therefore this difference observed in the first station (~20 h, Table 3.1) could be an indication of the upward movement and concentration of organisms in the upper layers.

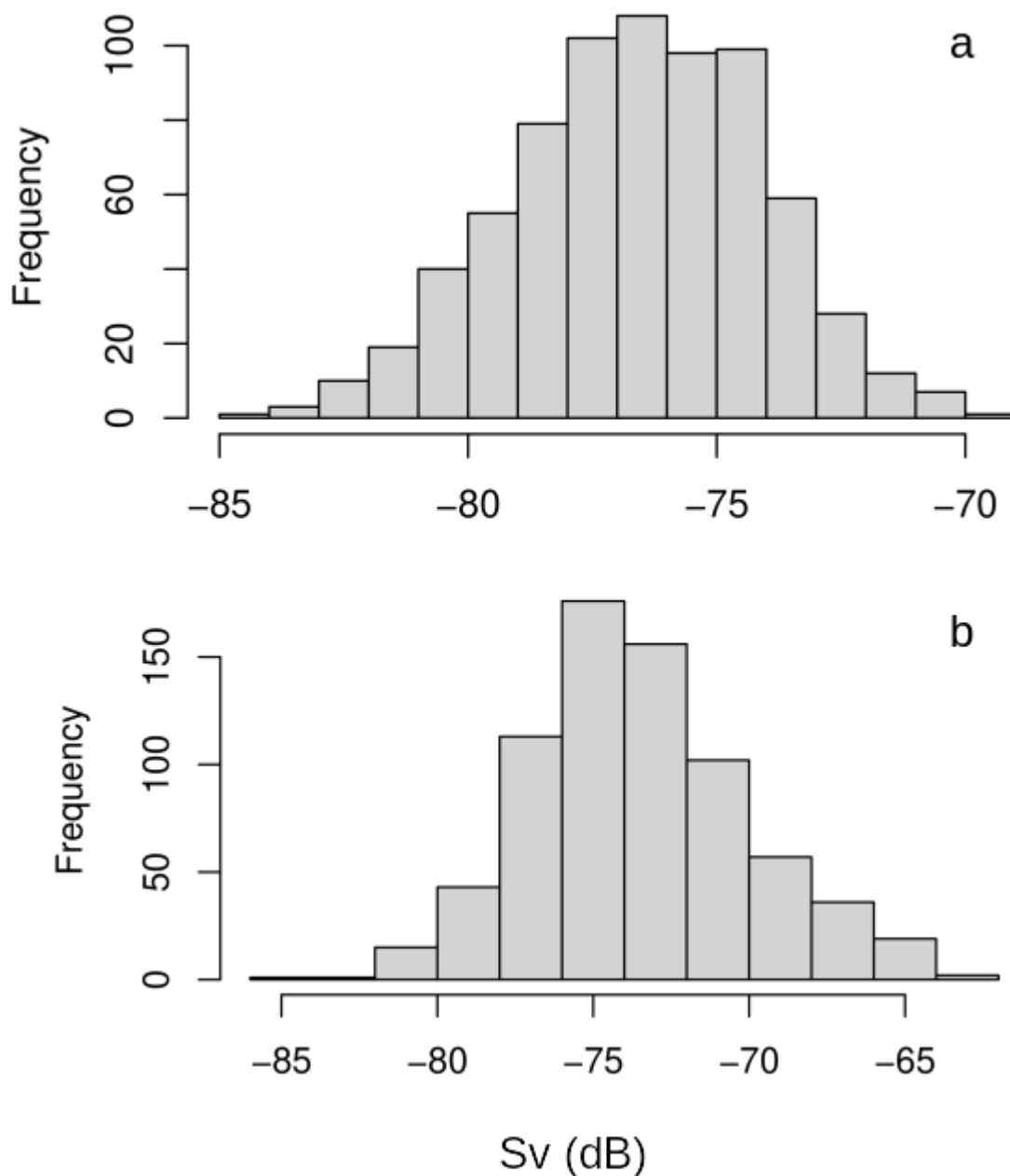


Figure 3.2.7: Distribution of acoustic backscatter (Sv(120kHz), dB) at station 438 detected by the submersible echosounder of the two mesopelagic layers observed, one at 350m (a) and another at 450m (b). Please note that the histogram a) and b) Y axes are not at the same scale.

MFRI will therefore work further to categorize the single target broadband acoustic measurements of macrozooplankton and nekton backscatter of DSML with the submersible echosounder during the 2021 Icelandic spring survey. Information on catch composition of mesopelagic organisms will be compared in more detail with observations of the acoustic backscatter layer obtained with the submersible echosounder and the findings will be compared the hull-mounted acoustics.

Contact person: Teresa Silva ([teresa.silva@hafogvatn.is](mailto:teresa.silva@hafogvatn.is))



### 3.2.3. DTU: Separation of fish and siphonophores through combined acoustic and optical measurements:

DTU: Better knowledge about the composition of the mesopelagic layers is needed (P2.2). There are several challenges in acoustic methods. Swimbladder resonance, swimbladder morphology, and erroneous inclusion of gelatinous zooplankton. Mesopelagic fishes have been proven difficult to separate acoustically from physonect siphonophores. Siphonophores are easily shredded in trawls and are difficult to sample (P2.4). By using lowered acoustic devices together with optics, single targets can become resolved and more thus more information about scattering properties, abundance and behaviour can be obtained.

By applying target tracking on data obtained with the system described in 2.2 (Fig. 2.2.1), full frequency spectrums  $TS(f)$  were obtained in situ from depths between 10-550 m with tracks resonant close to 70 kHz observed in a layer optically identified to be siphonophores, and tracks similar to estimated previously on mesopelagic fish (Fig. 2.2.1).

Separation of fish and siphonophores:

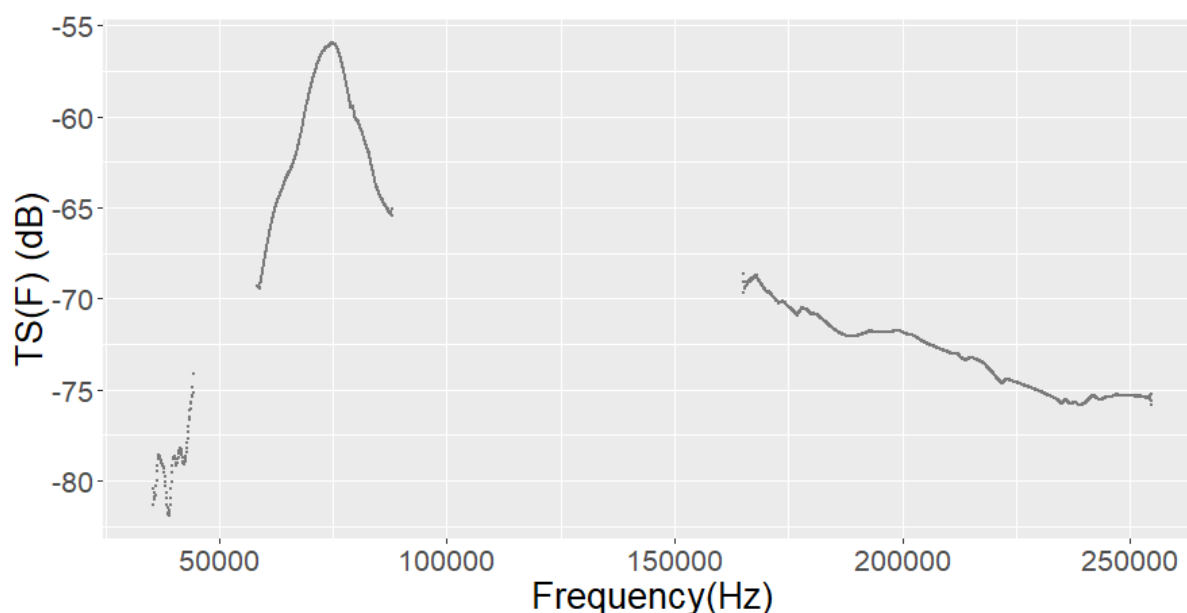


Figure 3.2.3. One frequency spectrum  $TS(f)$  for a track in a layer of visually identified siphonophores

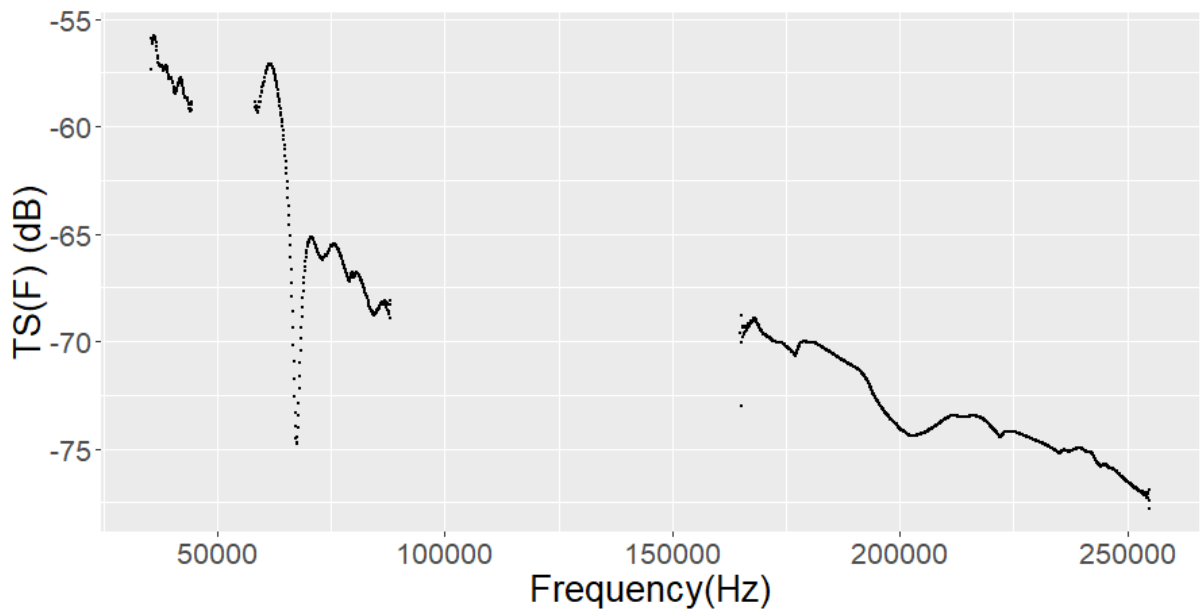


Figure 3.2.4. Track of target from the deep scattering layers, believed to be a mesopelagic fish, by comparing with previous literature.

### 3.3 Direct estimates of mesopelagic abundance based on echo counts

The traditional approach to converting the acoustic signal to abundances ( $S_1$ ) is to sum up the total amount of sound backscattered over a depth channel, and then divide by the average TS to arrive at an average density. However, it is immediately evident from e.g., Fig. 3.1 that individual scatterers can be identified and counted directly, with few assumptions needed. If the observation volume is known, it is trivial to convert these counts to densities (Fig. 3.1.1). The main assumptions needed are 1. that the observation volume is known, 2. that the organisms are detectable (e.g. signal strength above threshold and echo properties compliant with echo detection algorithm used) and 3. that the densities are low enough to allow separation of individual organisms. In practice the method is likely to be restricted to ranges close to the transducer, requiring the use of submerged acoustic equipment.

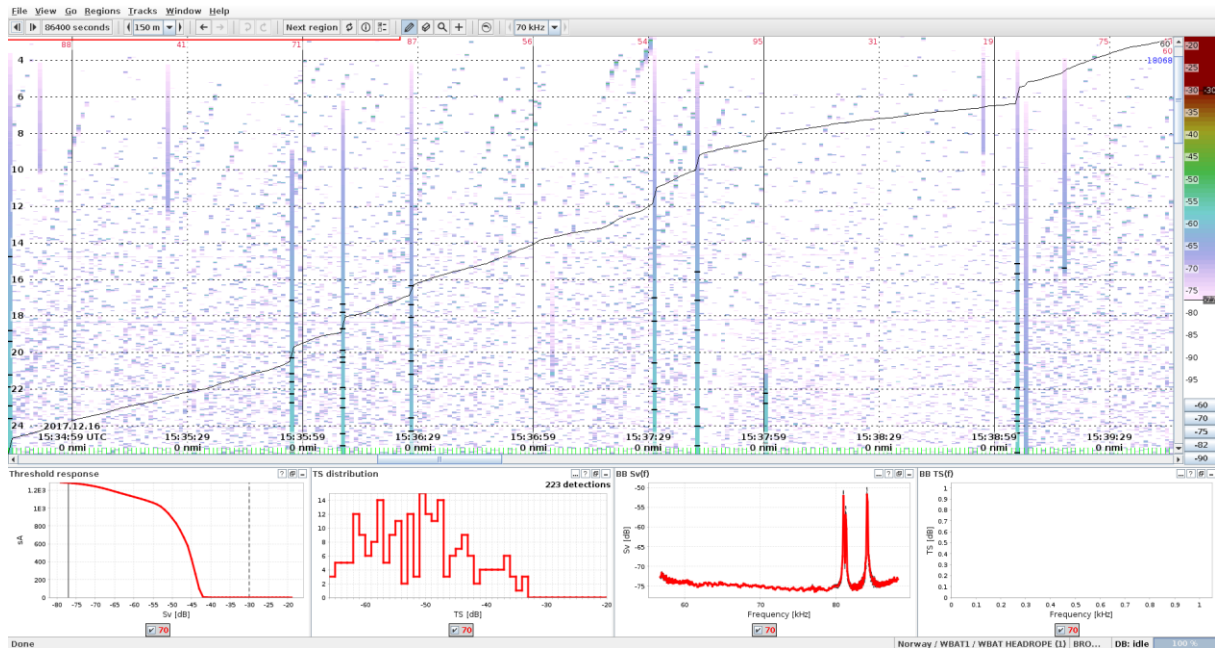


Fig. 3.3.1 70 kHz BB data collected from an autonomous, horizontally looking echosounder attached to the headrope of a trawl. Diagonal traces consist of single echoes from individual organisms approaching the trawl. Gaps in traces are caused by low ping rates, vertical bars are caused by interference from other trawl instrumentation.

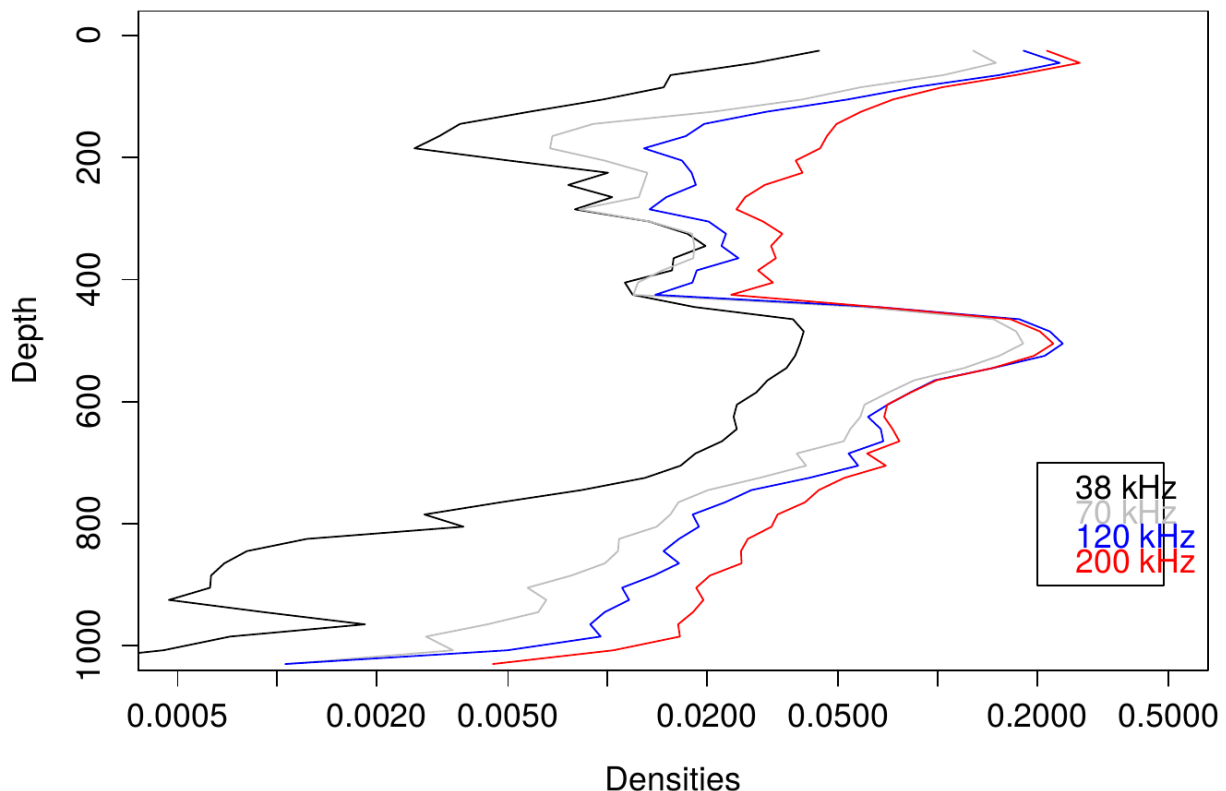


Fig. 3.3.2: Direct estimates of organismal densities from station 124, IMR cruise 2019703 (Fig. 3.1.1, 3.1.2), based on echo counts at 4 different frequencies. 38 kHz echoes were collected in CW mode, the other frequencies are based on FM data. 38 kHz echoes were detected at a lower threshold (e.g. densities at 38 kHz are based on stronger echoes), the echoes at the higher frequencies were all detected at the same absolute threshold.



IMR has during cruises aimed at studying the mesopelagic prioritised collecting acoustic data from resolved organisms, these data are our primary data-source for acoustic abundance estimates (S1) during these cruises. Most mesopelagic trawls during these cruises have attached a horizontally oriented echosounder on the headrope, providing a continuous record of individual scatterers ahead of the trawl opening. Due to ping-rate/data-range concerns these records have so far mostly been collected using a WBAT in CW mode (120/200 kHz). In addition, IMR has routinely deployed the MESSOR tow-body during these cruises (since 2018 38 kHz CW, 70 kHz FM, 120 kHz FM, 200 kHz FM), running the acoustics with settings optimized for collecting resolved echoes from single scatterers.

Contact person: Thor Klevjer (thor.klevjer@hi.no)



## 3.4 Improved parametrization of resonant scattering models

### 3.4.1 Direct/physical measurements that will improve our ability to parametrize models

#### Using X-Ray and magnetic resonance imaging to infer individual target strength of *M. muelleri* in the Northwest Atlantic

Determining the sound-scattering potential of individual fish is key /in order to convert acoustic abundances to biomass which is done by the use of species-specific target strength (TS) estimates. The swimbladder is the insonified bodypart of a fish which produces the large proportion of the acoustic backscatter. Therefore, it is crucial to know its specific morphology and dimensions which can then be used to derive realistic target strength estimates. Currently available target strength estimates have been derived from acoustic *in situ* and two-dimensional measurements taken from soft x-ray images of *M.muelleri* sampled from the Norwegian Sea (Scouling *et al.*, 2015) and the Bay of Biscay (Sobradillo *et al.*, 2019). We have opportunistically sampled *M.muelleri* from the North Atlantic (Irish Shelf region) during the Western European Shelf Pelagic Acoustic survey aboard the RV *Celtic Explorer*. Sampled fish were x-rayed and two-dimensional measurements were taken from the x-ray images (Figure 3.4.1). The imaged fish which displayed intact swimbladders were then taken for magnetic resonance imaging (MRI). The three-dimensional reconstructions of the three-plane MRI images of the swimbladder allows for a more accurate estimate of the swimbladder shape and volume (Fässler *et al.*, 2013). This is particularly important when considering the size of the fish and the fact that the TS estimates derived from two-dimensional x-ray images assumes that swimbladders are spheroid shaped. Consequently, the three-dimensional images of the swimbladder will allow for a more accurate target strength estimate. We are currently processing the MRI images.

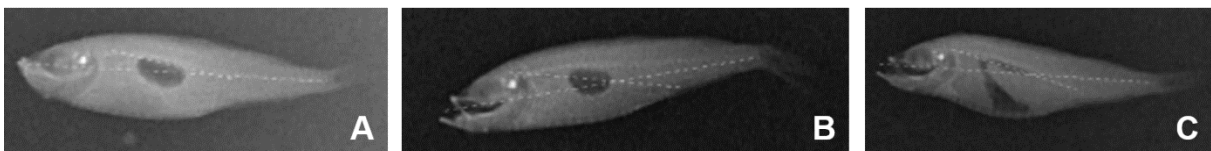


Figure 3.4.1: A and B show x-rax images of *M.muelleri* with intact swimbladders and C with a damaged and deflated swimbladder which was excluded in subsequent MRI analysis

### 3.4.2 Model implementations

#### Development of a backscattering model for *M. muelleri*

There are practical difficulties in acoustically assessing biomass of *M. muelleri* and other mesopelagic species, due to their small size and deep vertical distribution. One of the main difficulties is the nonlinearity of their individual acoustic response (or TS) according to changes in fish size and vertical location, the reason being the complex acoustic response of the fish swimbladder to the incident sound depending on the relation of the sound wavelength, the swimbladder volume and swimbladder membrane elasticity with changes in depth and fish size.

To try to overcome this problem, we are exploring a variation of the standard acoustic methodology applied on epipelagic species to consider this potential non-linearity in the abundance estimation process. The technique involves using a simple backscattering model to estimate the mean TS for a given range of fish lengths at each depth layer (rather than using one fixed single TS-length or TS-depth-length relation for the whole water column, as it is done for epi-pelagic species).

A recent study by Sobradillo *et al.* (2019) compared with empirical data a backscattering model for *M. muelleri* in two contrasted cases: (i) considering it as a physoclist species, i.e., allowing to compensate the swimbladder for pressure changes (and hence keeping a constant volume) and (ii) considering it as physostomous, i.e., forcing the bladder to compress with depth according to different grades of Boyle's law. This would have great implications in the interpretation of the swimbladder size measured on captured individuals (normally done with x-rays).

The result showed better fit when the model was applied considering pearlside as physostomous. This seemed to indicate that, during the trawls, pearlside is not able to compensate for pressure changes. But the study treated pearlside every time as a physoclist or every time as a physostomous. It did not allow the swimbladder to behave differently in natural migrations and in the trawls. To test this potential change of behavior, two variants of the model have been developed and will be tested against empirical data. In both variants, pearlside was simulated as a physostomous during the trawling process but then in natural migration it could behave as physostomous or physoclist or something intermediate.

The model tested was a classic and well-known resonant gas-bubble model adapted to ellipsoidal swimbladders (e.g., Andreeva, 1964; Scoulding *et al.*, 2015; Kloser *et al.*, 2016). It simplifies the acoustic response of the fish as the sole contribution of its swimbladder. The swimbladder was modelled using a variant of the gas-filled bubble backscattering model (Anderson, 1950) modified to account for ellipsoidal shape (Andreeva, 1964) and acoustic frequency directivity as in Scoulding *et al.* (2015). In our case, some of the parameters were changed, as well as a couple of equations, notably, allowing for two different types of swimbladder behavior depending on the situation: during the hauls, we applied a "stressed" pressure compression coefficient  $\alpha_{str}$  for the captured individuals; while during normal migrations, we used a "normal" coefficient  $\alpha_{norm}$ . Both coefficients can be optimized independently to the empirical data or they can be forced to have the same value.

The swimbladder shape was approximated as an ellipsoid of semi-major ( $a$ ) and semi-minor axes in the lateral ( $b$ ) and dorsal ( $c$ ) axes. These values were obtained from the morphological measurements based on the X-ray study made by Sobradillo *et al.* (2019) and then modified, assuming isotropic compression, according to:

$$V(z_{haul}) = \frac{4\pi}{3} abc (1 + 0.103 z_{haul})^{-\alpha_{str}} \quad (1)$$

where  $z_{haul}$  was the mean depth of the hauls where the X-ray samples were obtained (108.6 m) and  $\alpha_{stress}$  was adjusted to any real value between 1 (i.e., physostomous behavior: no swimbladder compensation and hence volume change by Boyle's law for a free bubble) and 0 (physoclist behavior: swimbladder compensation and hence no



volume change). The equivalent sphere radius  $a_{esr}$  at the mean haul depth (considered as a reference) was estimated accordingly as:

$$a_{esr}(z_{haul}) = (abc)^{1/3} (1 + 0.103 z_{haul})^{-\alpha_{norm}/3} \quad (2)$$

From here, to estimate the equivalent radius of the swimbladder at each depth, we applied:

$$a_{esr}(z) = a_{esr}(z_{haul}) \left( \frac{1 + 0.103 z_{haul}}{1 + 0.103 z} \right)^{-\alpha_{norm}/3} \quad (3)$$

Where, as we did with the stressed one, the  $\alpha_{norm}$  coefficient was allowed to vary from 0 to 1, i.e., as a physoclist as a physostome or as any possible intermediate state. The backscattering of pearlside was based on the model by Love (1978), corrected for the swimbladder elongation:

$$\sigma_{bs,z} = \frac{(\rho_w / \rho_f)^2 \chi^2 a_{esr}^2(z)}{\left[ 1 - \left( \frac{f_{res}}{f} \right)^2 \right]^2 + \delta^2} \quad (4)$$

where  $f_{res}$  is the resonance frequency of the swimbladder,  $f$  is the acoustic frequency,  $Q$  is the quality factor that accounts for radiation, viscous, and thermal processes, and  $\chi$  is the coefficient accounting for the amplitude enhancement due to swimbladder elongation (Ye, 1997), expressed as:

$$\chi = \frac{\varepsilon^{-2/3} (1 - \varepsilon^2)^{1/2}}{\ln \frac{1 + (1 - \varepsilon^2)^{1/2}}{\varepsilon}} \quad (5)$$

The resonance frequency was estimated as:

$$f_{res}(z) = \frac{C_e}{2\pi a_{esr}(z)} \sqrt{\frac{3\gamma_a P(z) + 4\mu_r}{\rho_f}} \quad (6)$$

where  $\varepsilon$  is the eccentricity of the swimbladder (i. e.,  $b/a$ ), is the ratio of the specific heat for air;  $P$  is the ambient pressure at depth,  $\mu_r$  is the real part of the rigidity of fish flesh, and  $\rho_f$  is the density of fish flesh. The elongation factor  $C_e$  was presented by (Love, 1978) based on the work of Strasberg (1953) and Weston (1967).

$$C_e = \frac{2^{1/2} (1 - \varepsilon^2)^{1/4}}{\varepsilon^{1/3}} \left[ \ln \left[ \frac{1 + (1 - \varepsilon^2)^{1/2}}{1 - (1 - \varepsilon^2)^{1/2}} \right] \right]^{-1/2} \quad (7)$$

The damping factor, can be expressed in terms of radiation, viscous and thermal components as in Love (1978):

$$\delta(z) = \delta_{rad} + \delta_{vis} + \delta_{th} \quad (8)$$



Being:

$$\delta_{rad}(z) = \frac{2\pi\rho_w f_{res}^2 a_{esr}(z)}{c\rho_f f(z)} \quad (9a)$$

$$\delta_{vis}(z) = \frac{4\mu_r\mu_i}{\pi\rho_w f(z)a_{esr}^2(z)} \quad (9b)$$

$$\delta_{th}(z) = \frac{3(\gamma_a - 1)}{2\pi f a_{esr}(z)} \left( \frac{\pi f \kappa_a}{\pi \rho_a c_{pa}} \right)^{1/2} \left( 1 + \frac{s}{2\pi^2 \rho_f f_{res}^2(z) a_{esr}^3(z)} \right)^{-1}, \quad (9c)$$

where  $k = 2\pi f/c_w$  is the acoustic wave number ( $c_w$  is the sound speed in water),  $\xi$  is the viscous coefficient,  $s$  is the surface tension at the fish flesh and swimbladder interface,  $\kappa$  is the thermal conductivity of air and  $c_{pa}$  is the specific heat at constant pressure for air. The angular dependency of the backscattering at or near the resonant frequency was included by using the next directivity function, given by Stanton (1988):

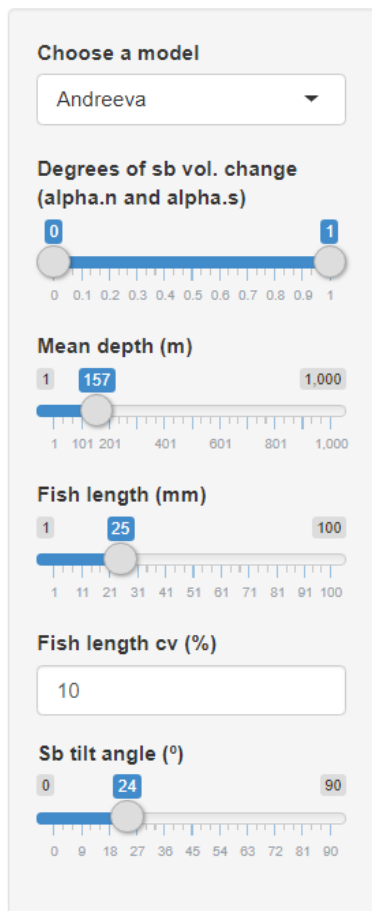
$$D_\theta = \frac{\sin\left(\frac{kL}{2\sin\theta}\right)}{\frac{kL}{2\sin\theta}} \quad (10)$$

Where  $k$  is the wave number,  $L$  is the length of the swimbladder, and  $\theta$  is the angle of orientation (is broadside incidence). Combining equations (4) and (10), we obtain:

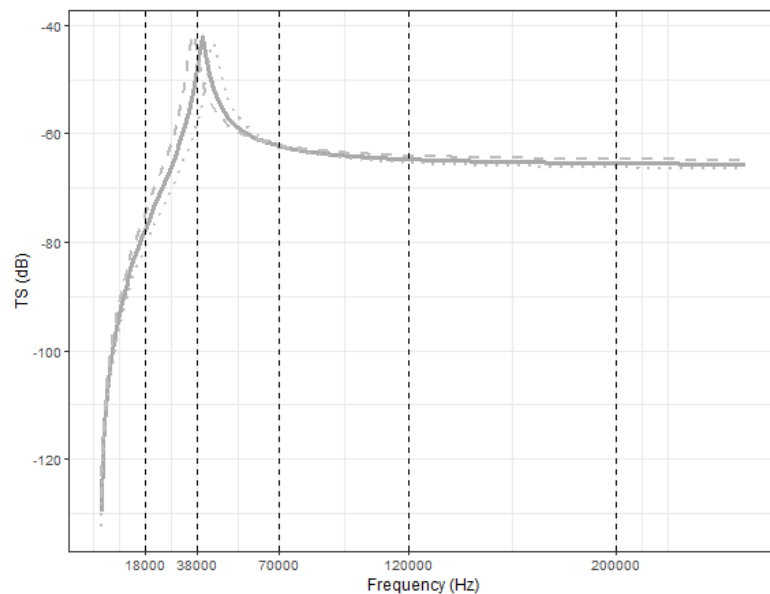
$$\sigma_{bs}^{total} = D_\theta \sigma_{bs} \quad (11)$$

Also, a sensitivity analysis of the target strength obtained with the scattering model to  $\alpha$  was performed, where  $\alpha$  ranged from 0 (no volume change) to 1 (Boyle's law volume change).

The model has been wrapped in a graphic user interface based on Shiny-R (Figure 2) to make it easier to use, particularly to facilitate underway comparisons against broadband frequency responses during acoustic surveys. Two types of analyses are being carried out to validate the model: First, the model variants will be checked again against the empirical values obtained in (Sobradillo *et al.*, 2019), this time explicitly considering the functional relationship with depth. In addition, further experiments are being conducted in JUVENA 2020 to further validate the models, trying to highlight the highest contrast between the different model variants. Contact person: Guillemo Boyra (gboyra@azti.es).



Predicted frequency response



Estimated swimbladder sizes at depth

Mean swimbladder length: 1.7 mm at 157 m depth  
 Mean swimbladder ESR: 0.39 mm at 157 m depth  
 Min swimbladder ESR: 0.35 mm at 157 m depth  
 Max swimbladder ESR: 0.43 mm at 157 m depth  
 (ESR: Equivalent Sphere Radius)

Figure 3.4.2. Shiny-R based graphic user interface of the backscattering model for Mueller's pearlside developed by AZTI.

### 3.4.3 Estimates of model parameters through model inversion

The swimbladder is a strong acoustic reflector and therefore a crucial component for quantitative analysis of acoustic data in fisheries acoustics. If misinterpreted, it can cause significant biases in biomass estimation. We (IMR) have used a modified version of the swimbladder model (Fig. 3.4.3.1) first introduced by Feuillade and Nero (1998) which is a two layers spherical viscous-elastic model. This mathematical/physical model includes not only the swimbladder, but also elastic tension of swimbladder-wall and the viscosity of surrounding flesh. Therefore, it better resembles the swimbladder compared to previous models.

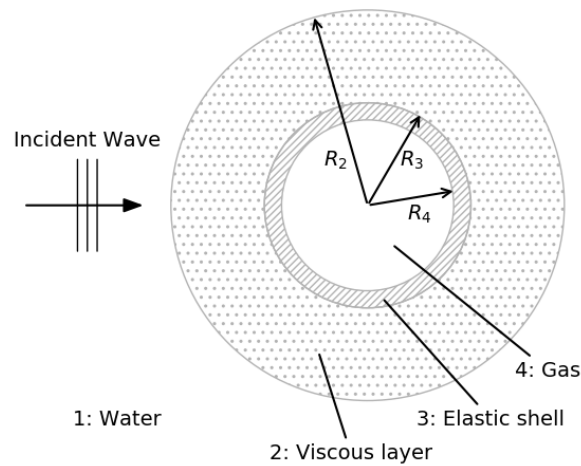


Fig. 3.4.3.1. Viscous-elastic model of spherical swimbladder (after Feuillede and Nero, 1998).

The model parameters are given in table below.

Model parameters	
<b>R2</b>	Equivalent spherical radius (ESR, mm)
<b>R3</b>	Radius (mm) of swimbladder including swimbladder wall.
<b>R4</b>	Radius (mm) of swimbladder excluding swimbladder wall.
<b><math>\rho</math>1</b>	Density (kg/m <sup>3</sup> ) of surrounding seawater (calculated using in situ measured temperature, salinity and pressure)
<b>c1</b>	Sound speed (m/s) in surrounding seawater (calculated using in situ measured temperature, salinity, and depth)
<b><math>\rho</math>2</b>	Density (kg/m <sup>3</sup> ) of fish flesh
<b>c2</b>	Sound speed (m/s) in fish flesh
<b><math>\mu</math>3</b>	Shear modulus (MPa) of swimbladder wall
<b>c4</b>	Sound speed (m/s) of gas inside swimbladder

Effects of different parameters on the TS frequency response are presented in Fig. 3.4.3.2. Base model (Line 0) is shown by the solid black line and its parameters are given in the lower left panel. The updated parameter compared to the base model are shown for lines 1-8 by different colors and line styles. For example, reducing the swimbladder size (Line 1), increasing the wall tension (Line 2), or wall thickness (Line 3) shifts the main resonance to a higher frequency. For further details see Khodabandeloo et al. 2021.



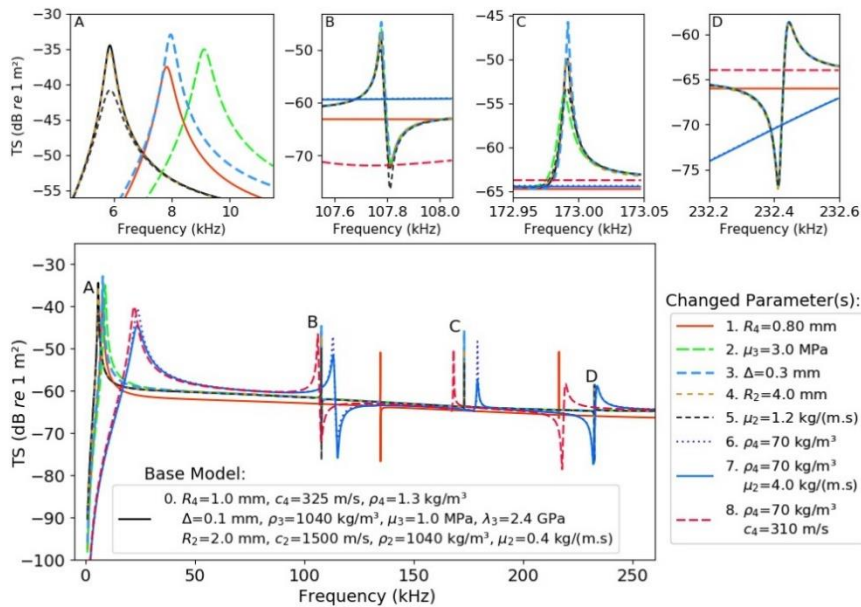


Fig. 3.4.3.2. Effects of different parameter variations on the target strength frequency response of viscous-elastic spherical swimbladder over the frequency range 1–260 kHz.

### 3.4.4 Inversion of scattering models for biomass estimation

The procedure for weight estimation from the collected acoustic data using the viscous-elastic backscattering model is shown in Fig. 3.4.4.1

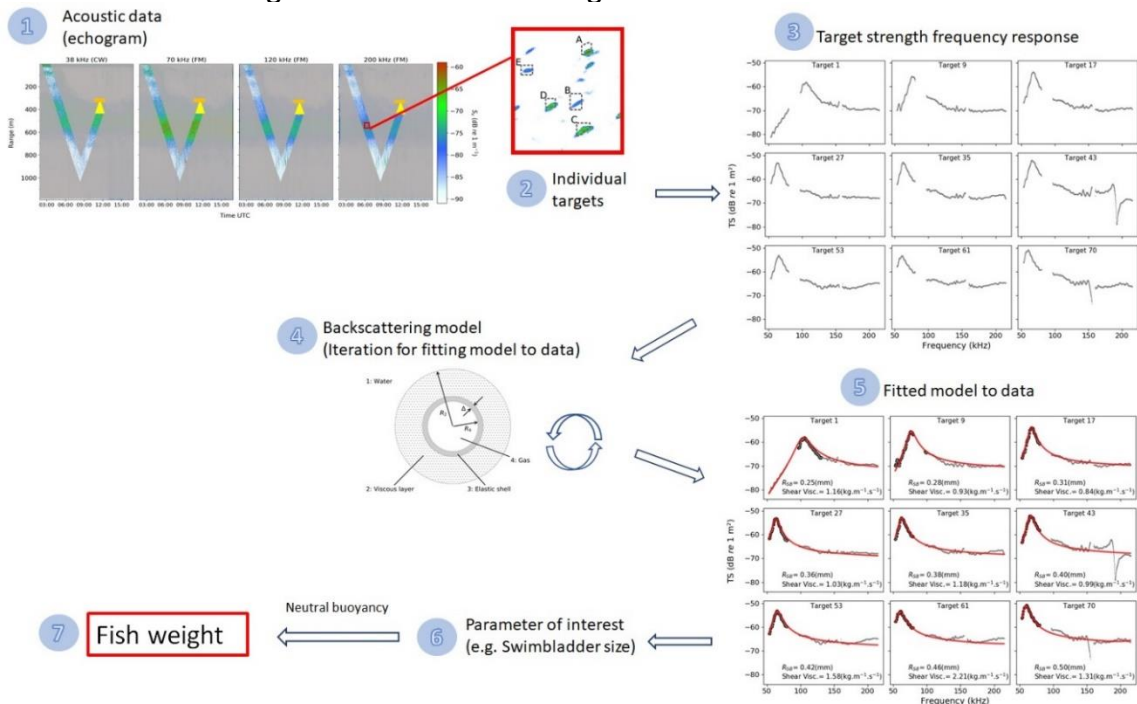


Fig. 3.4.4.1. Graphical summary of weight estimation from acoustic data using the backscattering model.

Using the above-mentioned procedure, the backscattering model is fitted to the TS frequency response of 12 single targets, and it shows a good agreement over the entire measured frequencies (Fig. 3.4.4.2). It is observed that the model captures peaks and nulls at higher frequencies as well as the main resonance.



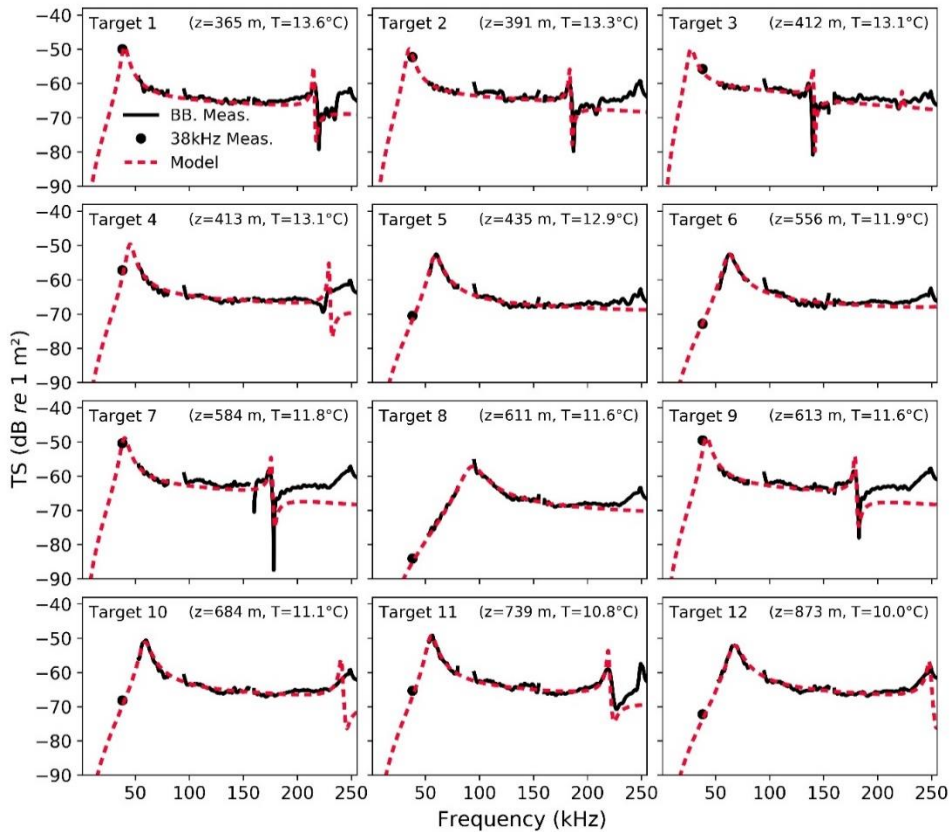


Fig. 3.4.4.2. Measured *in situ* (solid black line) and modeled (dashed red line) targets strength frequency responses for 12 selected individual targets.

Swimbladder radius, one of the model parameters, can be extracted from the fitted model and therefore size (i.e. volume) of the swimbladder can be estimated. By assuming neutral buoyancy of the fish, the fish weight can then be estimated. We've done this for stations sampled during the 2019 KPH cruise (cruise no. 2019703), and present results obtained during analysis from this cruise (see Agersted *et al.* (under review)). The catch data suggested that fishes of the genus *Cyclothone* dominated numerically and based on a combination of Multinet and trawl data, the numerical density by weight for *Cyclothone spp.* was estimated, along with the average weight per individual of *Cyclothone spp.*, (0.047 g).

Single targets were manually detected from the broadband acoustic data collected by MESSOR between 400 and 800 m (the depth of the *Cyclothone* layer), and these 822 unique targets were input to the resonant backscatter model (section 3.4.3), which under the assumption of overall neutral buoyancy was used to create an ensemble of fish weight distributions by varying the fish flesh density (a poorly known parameter for mesopelagic fish, but one with implications for overall scattering levels from resonant models).

When neutrally buoyant, the weight of the fish compensates for the buoyancy effect of the swimbladder:

$$(\rho_w - \rho_g) \times \frac{4}{3} \pi R_4^3 = W_f (1 - \rho_w / \rho_f), \quad (12)$$

Where  $\rho_w$  is water density,  $\rho_g$  is density of gas inside the swimbladder,  $\rho_f$  is fish flesh density,  $W_f$  is fish weight, and  $R_4$  is the radius (mm) of swimbladder excluding

swimbladder wall.  $\rho_w$  was estimated based on the *in situ* measured salinity, temperature and depth of the individual targets and was ranging between 1.029 and 1.031 g ml<sup>-1</sup>.

By matching the empirical size distribution from the catches with the model output, an estimate of fish flesh density was achieved. On the other hand, if this parameter is known or estimated independently, the method can use acoustic data to infer *in situ* size distributions.

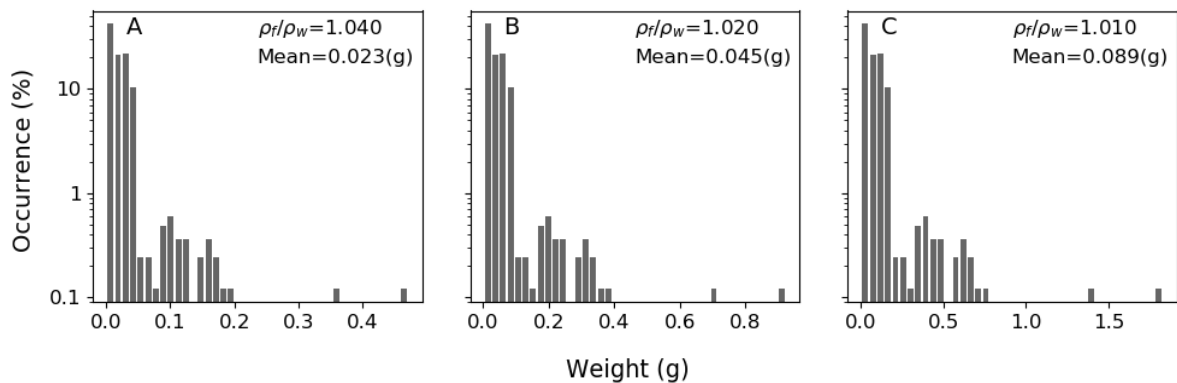


Figure 3.4.4.3. Weight distribution estimates of 822 targets using Eq.12 with three different fish flesh densities, resulting in different density contrasts ( $\rho_w/\rho_f$ ) displayed in each figure (A-C). Also, mean estimated weights (g) per individual found for each density contrast are listed in each figure, these ranges were compared with weight range estimated from net catches. Modified from Agersted *et al.* (under review).

For the model, a density contrast of 1.020 (fish flesh densities ranging from 1.047 to 1.049 g ml<sup>-1</sup>), resulted in high correspondence between weight-frequency distribution of fish from acoustics/model and for *Cyclothone* spp. in nets, with overall similar mean weights of individual fish estimated by the two different methods.

The weight estimate for each single target (Fig. 3.4.4.4) can then be summed in order to obtain the biomass of *Cyclothone* spp. from 400-800 m depth.

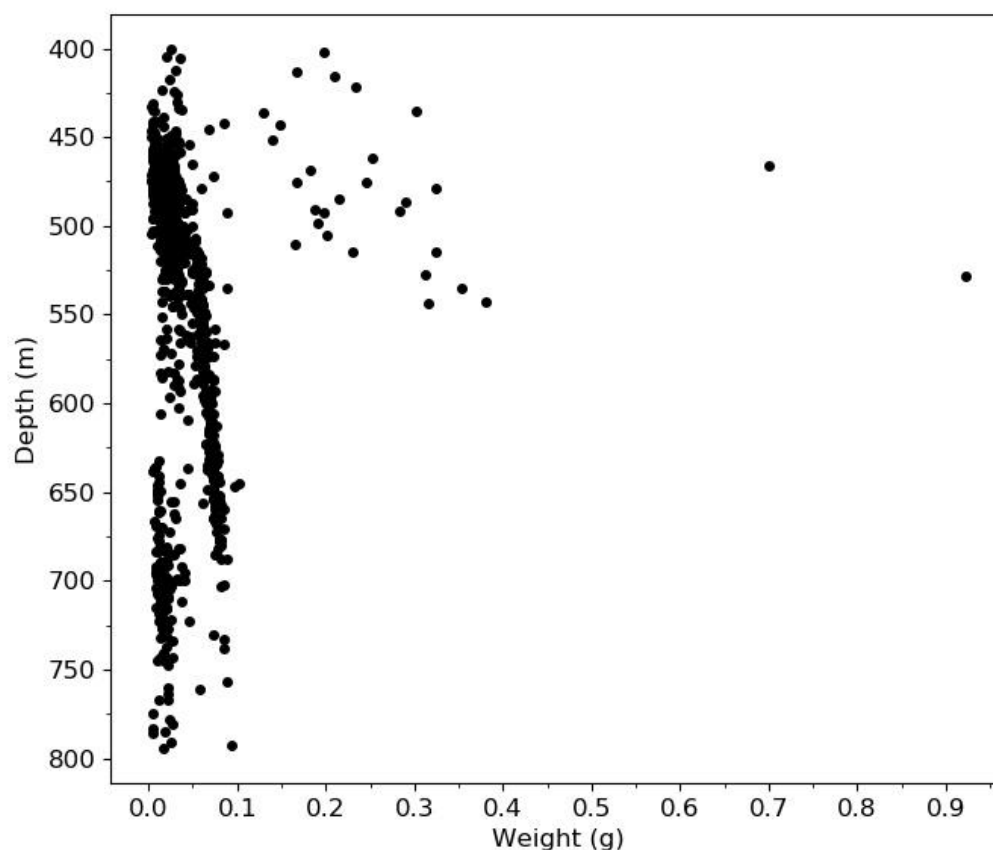


Fig. 3.4.4.4. Weight (g) estimated for all fish targets (n=822) assuming neutral buoyancy and applying a resulting density contrast  $\frac{\rho_f}{\rho_w} = 1.020$  (Error! Reference source not found.3B) (best fit compared to weight distribution from net catches; Fig. 3.4.4.3Error! Reference source not found.). Modified from Agersted *et al.* (under review).

## Conclusion/summary

Much of the work reported here has been focused on application of the relatively new acoustic broadband technology for measuring acoustic properties of mesopelagic organisms. The examples provided shows that this technology is promising when it comes to identifying (Chapter 3.2) and quantifying (Chapter 3.3) the abundance of mesopelagic organisms. The obtained results are directly useful when it comes to interpreting hull-mounted data, as well as for parametrization of acoustical models (Chapter 3.5), which again are useful for converting acoustic data from hull-mounted acoustic equipment to abundances. When it comes to converting acoustic data to actual biomasses with accuracy, we are however still very dependent on physical samples from trawls. For a few species, e.g. especially *Maurolicus muelleri*, the acoustic modelling is approaching a stage where it may allow accurate biomass estimates based on acoustic data (Chapter 3.4). This is in large part because *M. muelleri* has a behaviour that is somewhat atypical for a mesopelagic fish (e.g. shallow distribution and schooling); it is therefore in practice relatively easy to isolate in acoustic data. Inversion of BB acoustic data shows promise for biomass estimation (Chapter 3.4), but the method is at an early stage, and dependent on several conditions being met. While optical methods (Chapter 2) show some promise in identifying (and

measuring) especially fragile organisms, unknown magnitude of biases introduced by the need to get the optical devices close to the organisms (e.g. avoidance and attraction) make it hard to trust these data for general abundance and biomass estimates. Physical catches (Chapter 1) are therefore still essential for both taxonomic resolution and biomass estimates, as well as to interpret the acoustic data, even if trawling for mesopelagic organisms comes with its own set of biases and problems.

## References

Agersted, M. D., Khodabandeloo, B., García-Seoane, E., Klevjer, T. A., Strand, E., Underwood, M., and Melle, W. (under review). "Weight estimates of individual mesopelagic gas-bearing fish from in situ wideband acoustic measurements ground-truthed by net sampling."

Anderson, V. C. 1950. Sound Scattering from a Fluid Sphere. *Journal of the Acoustical Society of America*, 22: 426–431.

Andreeva, I. B. 1964. Scattering of sound by air bladders of fish in deep sound-scattering ocean layers. *Soviet Physics-Acoustics*, 10: 17–20.

Bassett, C., Lavery, A. C., Stanton, T. K., & Cotter, E. D. 2020. Frequency- and depth-dependent target strength measurements of individual mesopelagic scatterers. *The Journal of the Acoustical Society of America*, 148(2), EL153–EL158.

Benfield, MC; et al. 2003. "Distributions of Physonect Siphonulae in the Gulf of Maine and Their Potential as Important Sources of Acoustic Scattering." *Canadian Journal of Fisheries and Aquatic Sciences* [Can. J. Fish. Aquat. Sci./J. Can. Sci. Halieut. Aquat.]. 60 (7): 759–72.

Boyra, G., Martínez, U., Cotano, U., Santos, M., Irigoien, X., and Uriarte, A. 2013. Acoustic surveys for juvenile anchovy in the Bay of Biscay: Abundance estimate as an indicator of the next year's recruitment and spatial distribution patterns. *ICES Journal of Marine Science*, 70: 1354–1368.

Davison, P. C., Koslow, J. A., and Kloser, R. J. Acoustic biomass estimation of mesopelagic fish: backscattering from individuals, populations, and communities. – *ICES Journal of Marine Science*, doi: 10.1093/icesjms/fsv023

de Busserolles, F., Cortesi, F., Helvik, J.V., Davies, W.I., Templin, R.M., Sullivan, R.K., Michell, C.T., Mountford, J.K., Collin, S.P., Irigoien, X. and Kaartvedt, S., 2017. Pushing the limits of photoreception in twilight conditions: The rod-like cone retina of the deep-sea pearlshades. *Science advances*, 3(11). <https://doi.org/10.1126/sciadv.aao4709>

Douglas, R.H. and Partridge, J.C., 1997. On the visual pigments of deep-sea fish. *Journal of Fish Biology*, 50(1), pp.68-85.

FAO (Gjøsæter J, Kawaguchi K) (1980) A review of the world resources of mesopelagic fish. Food & Agriculture Org.



Fässler, S. M. M., O'Donnell, C., and Jech, J. M. 2013. Boarfish (*Capros aper*) target strength modelled from magnetic resonance imaging (MRI) scans of its swimbladder. *ICES Journal of Marine Science*, 70: 1451–1459.

Feuillade, C., and Nero, R. (1998). "A viscous-elastic swimbladder model for describing enhanced-frequency resonance scattering from fish," *The Journal of the Acoustical Society of America* 103, 3245-3255.

Giorli G, Drazen JC, Neuheimer AB, et al (2018) Deep sea animal density and size estimated using a Dual-frequency IDentification SONar (DIDSON) offshore the island of Hawaii. *Prog Oceanogr* 160:155–166. <https://doi.org/10.1016/j.pocean.2018.01.002>

Kaartvedt, S. 2010. Diel Vertical Migration Behaviour of the Northern Krill (*Meganyctiphanes norvegica* Sars). In *Advances in Marine Biology. The biology of Northern Krill*, pp. 255–275. Eds. Geraint A. Tarling and Michael Lesser. Elsevier Science.

Kaartvedt S, Staby A, Aksnes DL (2012) Efficient trawl avoidance by mesopelagic fishes causes large underestimation of their biomass. *Mar Ecol Prog Ser* 456:1–6

Khodabandeloo, B., M. D. Agersted, T. Klevjer, G. J. Macaulay, and W. Melle. 2021. Estimating target strength and physical characteristics of gas-bearing mesopelagic fish from wideband in situ echoes using a viscous-elastic scattering model. *J. Acoust. Soc. Am.* 149: 673–691.

Kloser, R. J., Ryan, T. E., Keith, G., and Gershwin, L. 2016. Deep-scattering layer, gas-bladder density, and size estimates using a two-frequency acoustic and optical probe. *ICES Journal of Marine Science*, pp. 2037–2048.

Korneliussen, R. J., Y. Heggelund, G. J. Macaulay, D. Patel, E. Johnsen, and I. K. Eliassen. 2016. Acoustic identification of marine species using a feature library. *Methods Oceanogr.* 17: 187–205. doi:10/gd3zvv

Kubilius R, Macaulay GJ, Ona E (2020) Remote sizing of fish-like targets using broadband acoustics. *Fish Res* 228:105568. <https://doi.org/10/gg9fzv>

Lam V, Pauly D (2005) Mapping the global biomass of mesopelagic fishes. *Sea Us Proj Newsl* 30:

Mauchline, J. 1980. *The Biology of Mysids and Euphausiids*. Academic Press, London and New York.

Moser, P.M., 1992. *Spectral Transmission of Light through Seawater*. Pacific-Sierra Research Corporation Warminster United States.

Love, R. H. 1978. Resonant acoustic scattering by swimbladder-bearing fish. *Journal of the Acoustical Society of America*, 64: 571–580.



Proud, R., Handegard, N. O, Kloser, R. J., Cox, M. J., Brierley, A. S., 2019. From siphonophores to deep scattering layers: uncertainty ranges for the estimation of global mesopelagic fish biomass, *ICES Journal of Marine Science*, 76(3), pp. 718–733.

Robison, Bruce H., Rob E. Sherlock, Kim R. Reisenbichler, and Paul R. McGill. 2020. “Running the Gauntlet: Assessing the Threats to Vertical Migrators.” *Frontiers in Marine Science* 7 (February): 64. <https://doi.org/10/ggpwvb>.

Rosen, S., Jørgensen, T., Hammersland-White, D., and Holst, J.C. 2013. DeepVision: a stereo camera system provides highly accurate counts and lengths of fish passing inside a trawl. *Canadian Journal of Fisheries and Aquatic Sciences*. 70(10): 1456-1467. <https://doi.org/10.1139/cjfas-2013-0124>

Rosen, S. and Holst, J.C., 2013. DeepVision in-trawl imaging: Sampling the water column in four dimensions. *Fisheries Research*. 148 64-73.

Scoulding, B., Chu, D., Ona, E., and Fernandes, P. G. 2015. Target strengths of two abundant mesopelagic fish species. *The Journal of the Acoustical Society of America*, 137: 989–1000.

Sobradillo, B., Boyra, G., Martinez, U., Carrera, P., Peña, M., and Irigoien, X. 2019. Target Strength and swimbladder morphology of Mueller’s pearlside (*Maurollicus muelleri*). *Scientific Reports*, 9: 1–14.

Stanton, T. K. 1988. Sound scattering by cylinders of finite length. I. Fluid cylinders. *Journal of the Acoustical Society of America*, 83: 55–63.

Strasberg, M. 1953. The Pulsation Frequency of Nonspherical Gas Bubbles in Liquids. *Journal of the Acoustical Society of America*, 25: 536–537.

Webb TJ, Vanden Berghe E, O’Dor R (2010) Biodiversity’s Big Wet Secret: The Global Distribution of Marine Biological Records Reveals Chronic Under-Exploration of the Deep Pelagic Ocean. *PLoS ONE* 5:e10223. <https://doi.org/10.1371/journal.pone.0010223>

Weston, D. E. 1967. Sound propagation in the presence of bladder fish. In *Underwater Acoustics*, pp. 55–88.

Ye, Z. 1997. Low-frequency acoustic scattering by gas-filled prolate spheroids in liquids. *The Journal of the Acoustical Society of America*, 101: 1945–1952.

## Supplementary information:

### Tables





Table 2.1: WBAT stations during JUVENA surveys 2019 and 2020

WBAT	Radial	Date	Time	Lat	Long
1	V11	24/09/2019	11:00	43.59	-3.45
2	V11	24/09/2019	12:00	43.59	-3.45
3	V11	24/09/2019	14:00	43.55	-3.44
4	V11	24/09/2019	14:21	43.55	-3.44
5	V11	24/09/2019	15:00	43.56	-3.50
6	V11	24/09/2019	15:55	43.56	-3.61
7	V11	26/09/2019	19:00	43.62	-3.47
8	V11	26/09/2019	19:57	43.58	-3.48
9	V11	27/09/2019	8:30	43.63	-3.48
10	V11	27/09/2019	8:53	43.63	-3.48
11	V11	27/09/2019	11:10	43.63	-3.48
12	V11V9	27/09/2019	19:01	43.56	-3.25
13	V11V9	27/09/2019	19:32	43.56	-3.25
14	V11V9	27/09/2019	21:25	43.56	-3.25
15	V9	28/09/2019	9:36	43.72	-3.21
16	V9	28/09/2019	15:56	43.58	-3.22
17	V16	11/09/2020	14:22	44.11	-4.42
18	v14	12/09/2020	18:00	43.57	-4.08
19	V8	17/09/2020	17:39	43.70	-3.04
20	D2	28/09/2020	13:49	45.16	-1.96
21	H2	29/09/2020	4:00	43.61	-1.52
22	H2	29/09/2020	6:30	43.61	-1.52

Table 3.1. Stations where the submersible echosounder (WBT-TUBE) was deployed during MFRI MEESO stations.

	Station	Date	Depth layer (m)	Location
MEESO1	438	24-07-2020, 19:26- 20:00	Layer 350 Layer 450	Irminger Basin
MEESO2	447	27-07-2020, 04:24-05:29	Layer 60 Layer 220 Layer 400	Iceland Basin
MEESO3	457	29-07-2020, 03:41-05:23	Layer 100 Layer 220 Layer 400	Iceland Basin
MEESO4	463	30-07-2020, 03:31-04:43	Layer 50 Layer 100 Layer 400	Off shelf south of Iceland



- Agersted, M. D., Khodabandloo, B., García-Seoane, E., Klevjer, T. A., Strand, E., Underwood, M., and Melle, W. (**under review**). "Weight estimates of individual mesopelagic gas-bearing fish from *in situ* wideband acoustic measurements ground-truthed by net sampling."
- Feuillade, C., and Nero, R. (**1998**). "A viscous-elastic swimbladder model for describing enhanced-frequency resonance scattering from fish," *The Journal of the Acoustical Society of America* **103**, 3245-3255.

